Alma Mater Studiorum – Università di Bologna

Dottorato di Ricerca In
Ingegneria Biomedica Elettrica e dei Sistemi

Ciclo 33

Settore Concorsuale: 09/G2 - BIOINGEGNERIA

Settore Scientifico Disciplinare: ING-IND/34 - BIOINGEGNERIA INDUSTRIALE

Development and Validation of a CO_2 Sensor for Extra Corporeal Life Support Applications

Presentata da:

Michele Bellancini

Coordinatore Dottorato:

Michele Monaci

Supervisore:

Emanuela Marcelli

Co-supervisore:

Stefano Severi

Esame Finale Anno 2021

Abstract

Measurement of carbon dioxide (CO_2) in medical applications is a well-established method for monitoring patient's pulmonary function in a noninvasive way widely used in emergency, intensive care, and during anaesthesia. Even in extra corporeal life support (ECLS) applications, such as Extra corporeal Carbon Dioxide Removal ($ECCO_2R$), Extra corporeal Membrane Oxygenation (ECMO), and cardiopulmonary by-pass (CPB), measurement of the CO_2 concentration in the membrane oxygenator exhaust gas is proven to be useful to evaluate the treatment progress as well as the performance of the membrane oxygenator. This thesis presents the development of a new optical sensor specifically designed for the measurement of CO_2 concentration in the oxygenator exhaust gas. The project's goal is to develop a sensor with Technology Readiness Level of 9, meaning that the developed sensor shall also be proven and validated in the operational environment. Initially, to allow a better comprehension of the application for which the developed sensor is intended, an overview of the ECLS application scenario is given, describing the key components of an ECLS device, as well as the most used ECLS procedures. Further, considerations about the importance of CO_2 concentration measurement in the membrane oxygenator exhaust gas are reported. Then, the measurement principle for carbon dioxide concentration is described, as well as state-of-the-art technologies used in this field. Moreover, design requirements that the developed sensor should meet are analyzed and disclosed. Sensor architecture is described, focusing on the method implemented to prevent condensation of the water vapour in the membrane oxygenator's exhaust gas. Effects of temperature on the performance of sensor's optical elements are addressed through theoretical and experimental analysis, and methods to avoid signal–temperature dependency are described. Finally, the results of the test performed on the developed sensor, both in-vitro and in-vivo conditions, are reported and discussed.

Acknowledgements

The research contribution presented in this Industrial PhD thesis has been funded by MediCon Ingegneria Srl through an "High Apprentice" contract position.

Contents

List of Figures

List of Tables

Chapter 1

Introduction

Capnometry is the measurement of carbon dioxide (CO_2) concentration in respiratory gases [1]. It is a well-known and established method for monitoring patient's pulmonary function in a non-invasive way, widely used in emergencies, in intensive care, or during anaesthesia [2, 3, 4, 5]. Even if the traditional use of capnometry is related to the field of respiratory monitoring, the application of this measurement in extra corporeal life support (ECLS) applications has been proposed. ECLS is defined as a set of therapies that focus on oxygenation, carbon dioxide removal, cardiac support, or a combination thereof [6]. Therefore, ECLS is used to treat those patients with cardio-respiratory failure refractory to maximal conventional treatment [7]. This support may facilitate therapeutic intervention, bridge to recovery, bridge to a long-term support device, heart or lung transplantation, or bridge to palliation. Recent research and development have transformed ECLS, which is now being delivered at an increasing frequency to patients globally. The increasing diffusion of ECLS is confirmed by the yearly report of Extra Corporeal Life Support Organization (ELSO) [8], to which Figure 1.1 refers.

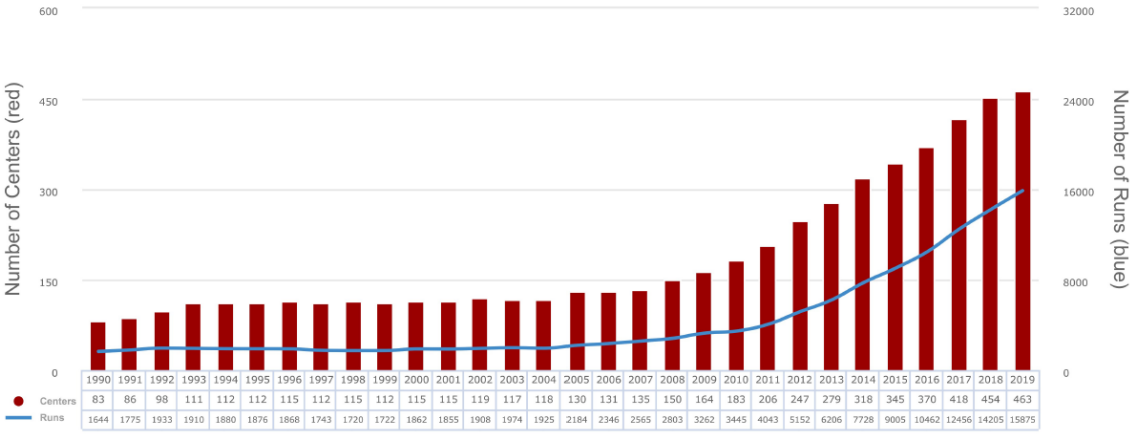

Figure 1.1: The trend of ECLS Runs and ECLS Centers from 1990 to 2020.

As shown on Figure 1.1, over 30 years ECLS procedure runs per year has increased from 1644 runs in 1990 to 15875 runs in 2020. Further, not only the number of runs per year has increased, but also the number of centres equipped to perform ECLS procedures (from 83 centres in 1990 to 463 of 2020).

Considering the increasing importance of ECLS as life-saving procedures, the development of devices and sensors for ECLS application is becoming more critical. Even though the use of capnometry in ECLS applications has been demonstrated useful to improve safety and effectiveness of the extra corporeal procedure, it is still not a routine measurement, primarily due to the lack of measuring systems specifically designed for ECLS applications. From this consideration comes the goal of this Industrial PhD, which is the development of a carbon dioxide sensor specifically designed for ECLS applications. The developed sensor provides the physicians and perfusionists information about CO_2 clearance during the ECLS procedure, which is useful to enhance both safety and effectiveness of the extra corporeal procedure. Further, this PhD project's goal is the development of a sensor with Technology Readiness Level (TRL) of 9 [9], meaning that the developed sensor shall also be proven and validated in the operational environment. To give a better comprehension of the application in which the developed sensor is used, in this chapter are disclosed the key components of an ECLS device and the most used ECLS procedures. Finally, the importance of CO_2 monitoring in ECLS application is discussed.

1.1 Key components of ECLS devices

In ECLS procedures, the functionality of the heart and lungs are temporally taken over by external devices. In particular, the main components of an ECLS device are:

- blood pump;
- extra corporeal oxygenator

1.1.1 Blood Pumps

In ECLS devices, a blood pump is used to substitute, partially or totally, the heart's functionality as the generator of the blood flow. In ECLS applications, two kinds of blood pumps are used:

- roller pumps,
- centrifugal pumps.

Roller pumps, or peristaltic pumps, comprise a length of PVC or silicone tubing situated against a curved metal backing plate (raceway) compressed by two rollers located on the ends of rotating arms at 180° to each other. The direction of compression of the tubing by the rotating arm containing the roller permits forward blood flow. Hence, this type of pump is described as a positive displacement device, allowing continuous delivery of blood volume despite variations in the outlet afterload. In roller pumps, blood flow depends upon the pump tubing internal diameter, rotation rate of the rollers and diameter of the pump head [10]. The following figure shows the principle of operation of a roller pump.

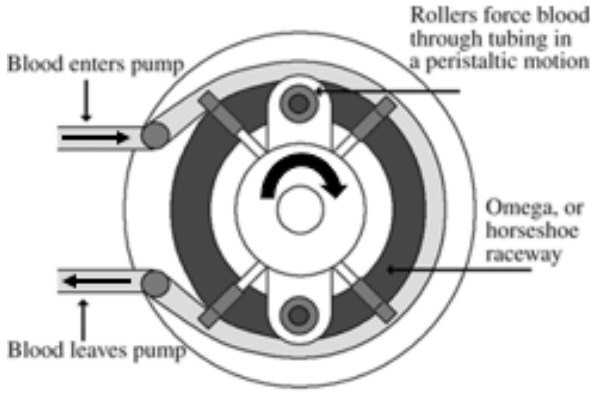

Figure 1.2: Schematic representation of a blood roller pump principle of operation.

Roller pumps are afterload independent, meaning that the increase of resistance downstream the pump does not affect the blood flow generation. Therefore, flow generation depends only on revolution per minutes (RPM) of the pump head, allowing simple monitoring of the pump functionality. Nevertheless, monitoring pressure downstream the pump is necessary to avoid circuit breakage due to the excessive pressure generated by the pump in case of tube occlusion. Further, roller pumps are defined as occlusive pumps since the constant presence of a roller that pushes on the tube wall prevents backflow in case of pump stop. Finally, roller pumps are versatile since they allow to change the flow direction if needed, changing the rotation sense of the pump head [11]. The main disadvantage of roller pumps is represented by blood damage due to high shear rates induced in the rollers' vicinity during occlusion, particularly during the reopening of the tubing once the roller has passed. During reopening, there may be momentary backflows with very high velocities. High shear on the cell membranes can lead to premature ageing of the red blood cells, which leads to clumping, and in extreme cases, to hemolysis of the red blood cells, releasing haemoglobin into the plasma [12]. However, roller pumps are still used, especially in short-term ECLS procedures such as cardiopulmonary by-pass (CPB).

Centrifugal pumps generate blood flow through the "vortex" effect. Within a plastic case (pumping chamber) a rotating body (impeller) generates a low-pressure zone at the centre of the pumping chamber, in which the blood is withdrawn, and a

high-pressure zone at the peripheral of the pumping chamber, from which the blood is ejected.

Figure 1.3 shows the principle of operation of a centrifugal pump.

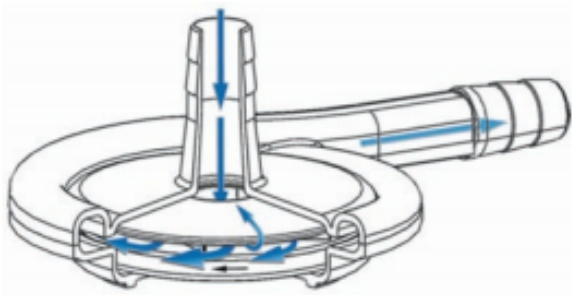

Figure 1.3: Schematic representation of a blood centrifugal pump principle of operation.

Generated blood flow depends on RPM of the rotating body and pressure drop across the pump. Therefore, unlike roller pumps, a variation of the resistance downstream the pump leads to significant variation of the generated blood flow. Therefore, due to dependency on the afterload, a direct measuring of the blood flow downstream the centrifugal pump to assure correct perfusion of the patient is necessary. An ultrasonic flow sensor is often used for this purpose. Centrifugal pumps are defined as non-occlusive pumps, since blood can pour in both directions, according to the pressure gradient, if the pump is stopped. The main advantage of centrifugal pumps compared to roller pumps is the lower hemolysis produced by the pump action. Centrifugal pump action is less traumatic for blood cells since there is no direct friction of the impeller with the pump housing, and free blood paths are present. However, the presence of turbulence or stagnation area within the pump may lead to high shear stress, hemolysis or thrombus formation. Impeller used in centrifugal blood pumps contains a magnet at the base. This magnet is used to couple the impeller to an electrical motor that generates the rotation force. Depending on the method used to generate the impeller rotation, centrifugal pumps can be divided in:

- magnetic rotation centrifugal pump and,
- magnetic levitation centrifugal pump.

Magnetic rotation centrifugal pumps are composed of a magnetic impeller coupled with a magnet placed on an external rotor. Rotation of the rotor element leads to rotation of the impeller within the pumping chamber. In order to maintain the impeller at the centre of the pumping chamber and avoid friction with the pump housing, shaft and bearings are necessary (Figure 1.4). However, the presence of shaft and bearings within the pump housing represents a discontinuity in the blood path, leading to turbulence and stagnation, thus increasing the risk of hemolysis and thrombus formation. Despite the presence of turbulence and stagnation area, magnetic rotation centrifugal pumps are anyway characterized by lower hemolysis rate than roller pumps [13].

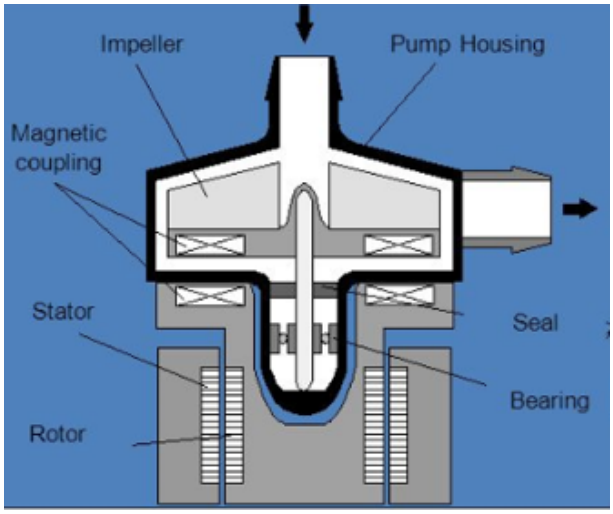

Figure 1.4: Schematic representation of a magnetic rotation centrifugal pump.

In magnetic levitation centrifugal pumps, the impeller's positioning and rotation are achieved through electromagnetic coupling of a magnet within the impeller and a magnetic field generated by electrical currents flowing in windings placed on an external stator. Since the impeller within the pumping chamber levitates and is maintained in a central position by the generated magnetic field, there is no need of shaft or bearings, and therefore within the pumping chamber, there is no discontinuity on the blood paths. (Figure 1.5) . Magnetic levitation centrifugal pumps represent the best solution in terms of hemolysis rate.

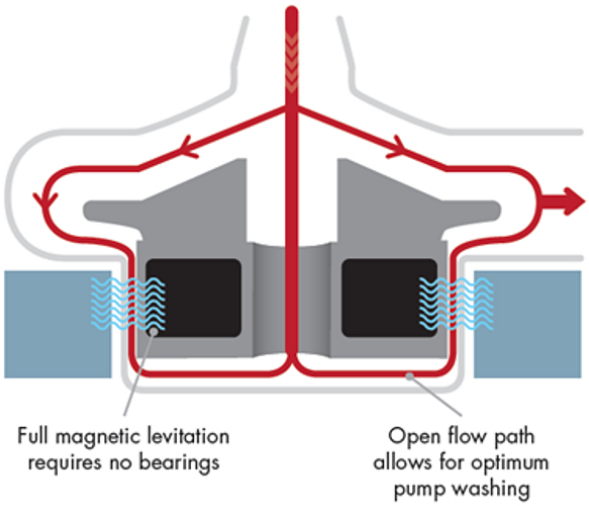

Figure 1.5: Schematic representation of a magnetic levitation centrifugal pump

1.1.2 Extra corporeal Oxygenator

To temporally substitute the lungs' functionality, an extra corporeal oxygenator, also known as artificial lung, is used in ECLS procedures. As a substitute of the patient's lungs, an oxygenator's purpose is to replace the organ gas exchange function during extra corporeal circulation, assuring both blood oxygenation and carbon dioxide removal [14]. There are different possibilities for blood-gas interaction: blood can be fed to a gaseous phase as in film oxygenator (obsolete in clinical practice), gas can be added to blood as in bubble oxygenator (rarely used anymore), or blood and gas can be separated by a membrane (nowadays membrane oxygenator).

In membrane oxygenator (MO), blood and gas compartments are divided by a membrane that is permeable to gas transfer. [15]. Venous blood enters the oxygenator, while gas (sweep gas) is also provided to the MO. Inside the MO gas exchange occurs, O_2 is added to blood while CO_2 is removed. Oxygenated blood then exits the MO returning to the patient's, while removed carbon dioxide is released in the atmosphere as exhaust gas. Therefore, in MO are present four connectors: blood inlet, blood outlet, gas inlet and gas outlet. In order to improve gas exchange, blood and sweep gas flows in a perpendicular direction. The membrane of modern MO can be divided into two categories: diffusion membrane (made of silicone) and microporous membrane. The second category is the most used nowadays. While diffusion

membrane is made of semi-permeable material that allows only the gas to move to the blood compartment and not the contrary, microporous membrane consists of hollow fibres with 0.05–0.3 μm pores that initially create a direct blood gas interface until a thin protein film quickly forms, producing molecular membranes. The gas exchange occurs by diffusion of the gases across microporous fibre surface, oxygen moving from the interior of the hollow fibre into the blood and carbon dioxide diffusing from the blood cross into the interior of the fibre and swept away by the gas flow through the hollow fibre [16]. Since the membrane surface is hydrophobic and the pores are small, no ultrafiltration of water occurs and gas and serum remain separated. Figure 1.6 shows the layout of a membrane oxygenator and its working principle.

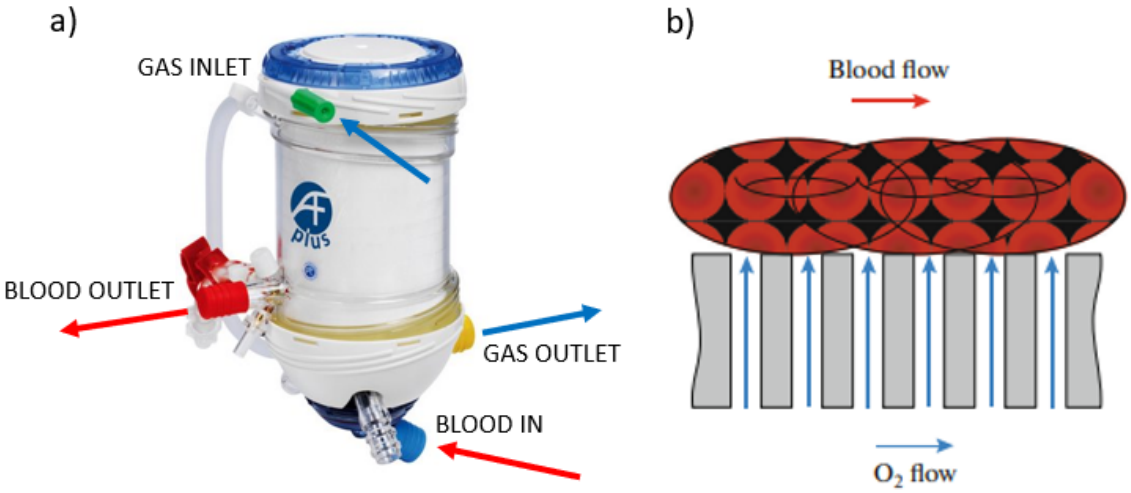

Figure 1.6: a)Microporous membrane oxygenator. b)Working principle schematic of a microporous membrane oxygenator.

In membrane oxygenators, gas transfer is achieved by diffusion as described by the Fick's Law:

$$V_{\text{gas}} \propto \frac{AD\delta P}{T} \tag{1.1}$$

where: V_{gas} [ml/min] is the gas flow across the membrane; A [m^2] is the membrane area; D [m^2/s] is the diffusion constant (that depends on the gas molecule of intrest) δP [mmHg] is the partial pressure difference (that represent the concentration gradient) across the membrane; ad T [m] is the membrane thickness. Equation 1.1

highlights that to increase gas transfer efficiency, blood-gas contact area shall be as larger as possible. Microporous membrane oxygenators are composed by a bundle of porous hollow fibres made of polypropylene or polymemethylpentene (PMP) and offer a more extensive exchange area than silicone membrane oxygenator. Nevertheless, is important to highlight that in membrane oxygenator the exchange surface area is 1.7-3.5 m^2 compared with 70-100 m^2 of natural lungs, while diffusion distance in MO is around 200 μm compared to the 10 μm of the human alveolus. Therefore, artificial lungs can not wholly substitute natural lungs in terms of gas exchange performance. The gas transfer also depends on the diffusion gradient across the membrane. Considering that the gas provided to the oxygenator is saturated with oxygen, for O_2 the partial pressure difference is 760 mmHg minus the O_2 tension of venous blood, while for CO_2 is equal to the carbon dioxide tension in venous blood. Despite the pressure gradient for O_2 is higher than the pressure gradient for CO_2, the material of the membrane oxygenator is more permeable to CO_2 than O_2 [17]. Even though the membrane of MO is made of a hydrophobic material, over time, adsorption of plasma proteins creates a hydrophilic passage on the micropores of the membrane. This leads to movement of liquid through the micropores from the blood to the gas side of the membrane, this phenomenon is called plasma leakage [18]. In practice, plasma leakage results in deterioration of gas exchange and gross leakage of plasma [19]. PMP membrane oxygenators are characterized by significantly less plasma leakage and a longer functional lifetime, up to several weeks [20]. Reduction of gas exchange capability may also result from clot formation on the membrane, which decreases the available surface area for gas exchange, and excess condensation in the membrane lung ("pulmonary oedema") [21]. The causes mentioned above may lead to MO failure and, therefore its replacement.

1.2 ECLS procedures

Even though all ECLS procedures involve blood pumps and membrane oxygenators, several different ECLS procedures exist, which differs for therapeutic goal, duration and kind of support provided to the patient. In this section, the below listed ECLS

procedure are described:

- Cardiopulmonary by-pass (CPB)
- Extra corporeal Membrane Oxygenation (ECMO)
- Extra corporeal CO_2 Removal (ECCO2R)

1.2.1 Cardiopulmonary by-pass - CPB

Cardiopulmonary by-pass, or CPB, is a form of extra corporeal circulation that redirects the patient's blood from venae cavae directly to the aorta, therefore by-passing both heart and lungs. The CPB procedure's goal is to provide a bloodless field to cardiac surgery, necessary for "open heart" surgical operations. During the surgical operation, the heartbeat is stopped, CPB circuit allows both circulatory and respiratory support along with temperature management [22]. CPB procedure is managed through a device called Heart-Lung Machine (HLM), which is composed of both disposable components and hardware and electronic devices. The main components of HLM are:

- Venous Reservoir
- Systemic Pump
- Membrane Oxygenator
- Cardioplegia System
- Cardiotomy Suction System

Figure 1.7 shows the schematic of a cardiopulmonary by-pass system [23].

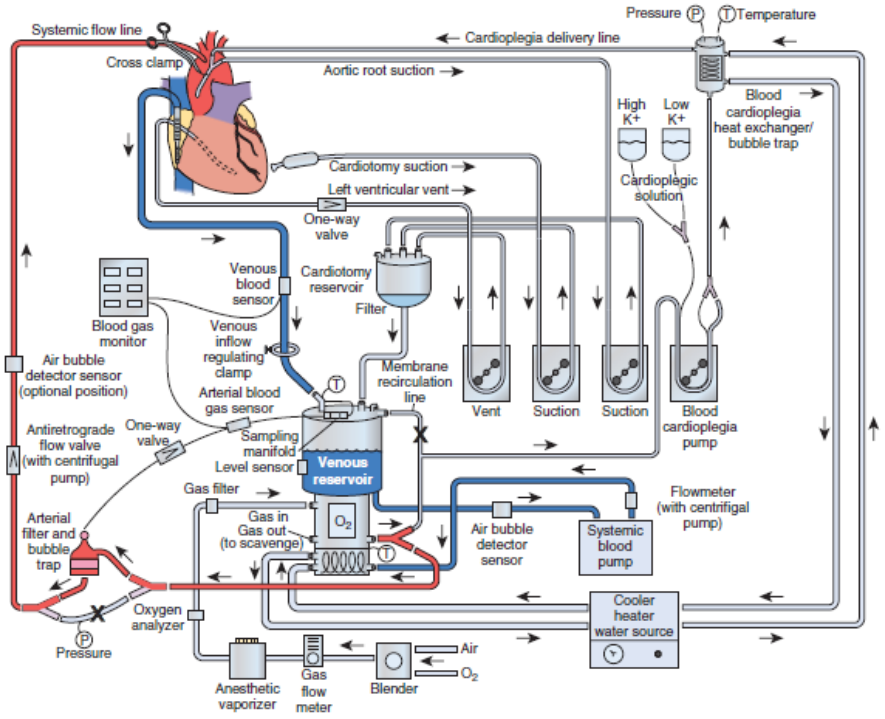

Figure 1.7: Schematic of a cardiopulmonary by-pass system

Patient's venous blood is collected in the venous reservoir that serves as a mixing chamber for all blood returning (e.g. cardiotomy and cardioplegia circulation). Further, the venous reservoir is filled by gravity. Therefore, it is usually placed below the patient's level; in this way, the patient is decoupled from the systemic pump, preventing excessive suction. The systemic pump acts as an artificial heart by pulling the blood from the venous reservoir and directing it towards the membrane oxygenator and then back to the patients through the aorta [24]. Both centrifugal and roller pumps are used as systemic pump. Roller pumps, even though more hemolytic, results suitable due to the "short-term" nature of the CPB procedure since the surgical procedure's duration is in the order of hours. In the membrane oxygenator, venous blood is oxygenated, and carbon dioxide is removed, obtaining arterial blood that is returned to the patient. Cardioplegia system can be considered as an additional circulation line, in which blood is withdrawn from the extra corporeal circuit (e.g. from the venous reservoir) and mixed with cardioplegia solution. Cardioplegia solution is a pharmaceutical solution that stops the heartbeat when mixed with blood and provided to the myocardium. Usually, potassium-based cardioplegia solution

is used, since allows the heart to stop during the diastole phase, meaning that the heart tissue is relaxed and therefore easier to manage during the surgical procedure [25]. Considering the small amount of blood volume processed by the cardioplegia system, roller pumps are commonly used for this purpose. Cardiotomy suction system is composed of roller pumps that withdraw the blood from thoracic cavity and blood that is returned directly to the heart (e.g. through the Tebesio veins), and return it to the venous reservoir. The cardiotomy suction system allows to obtain a bloodless surgical field and not waste blood produced by surgical operations. However, cardiotomy suction blood contains fat, bone, lipids, and other debris from the surgical field. This blood is also exposed to air, shear forces, and artificial surfaces that cause exacerbation of the systemic inflammatory response and result in microcirculatory dysfunction. These substances are dangerous if delivered to the patient; therefore cardiotomy suction blood is treated through dedicated filters [26].

1.2.2 Extra corporeal Membrane Oxygenation - ECMO

Extra corporeal membrane oxygenation, or ECMO, is used for the management of life threatening pulmonary or cardiac failure (or both), when no other form of treatment has been or is likely to be successful. It is used as temporary support, usually awaiting recovery of organs. ECMO is essentially a modification of the cardiopulmonary by-pass circuit which is used routinely in cardiac surgery. Blood is removed from the venous system either peripherally via cannulation of a femoral vein or centrally via cannulation of the right atrium, oxygenated, has its carbon dioxide extracted and then returned back to the body, either peripherally via a femoral artery or centrally via the ascending aorta [27]. Unlike CPB, native lungs and heart are not entirely excluded from the circulation, but instead, the artificial heart (pump) and lungs support the native organs during their recovery. The primary ECMO circuit consists of a blood pump, the membrane oxygenator, conduit tubing, a heat exchanger, and drainage and return cannulae. The circuit drains blood from the venous system and pumps it through a membrane oxygenator where O_2 is added, and CO_2 is removed, returning newly oxygenated blood to the patient [28]. Depending on the cannulation configuration used, ECMO can provide circulatory

and respiratory support or only respiratory support. Venoarterial ECMO (VA-ECMO) is able to provide both respiratory and circulatory support. Deoxygenated blood is drained from the venous system, and oxygenated blood is returned into the arterial circulation, in a similar fashion to standard cardiopulmonary by-pass. The pulmonary circulation is by-passed by placing the artificial lung in parallel with the native lungs [29]. Venovenous ECMO (VV-ECMO) is intended to provide partial or complete respiratory support without any cardiac support, so VV-ECMO is indicated only when native cardiac output is sufficient. VV-ECMO places the native lungs in series with the artificial lung. In adults, several cannulation options currently exist. Traditionally, deoxygenated blood is drained from a femoral vein and returned to the right internal jugular vein [30]. More recently, a bicaval dual-lumen catheter has been developed to provide both drainage and return directly into the right atrium via the internal jugular vein [31]. In the following figure, a schematic representation of VA-ECMO and VV-ECMO is reported.

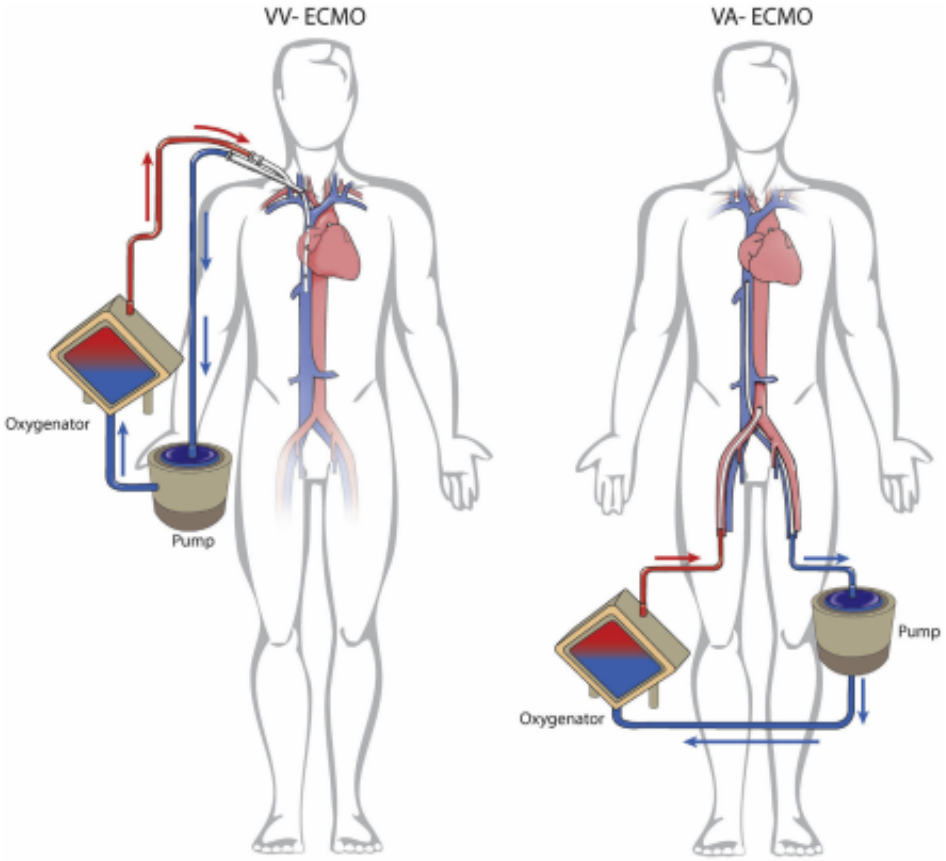

Figure 1.8: Schematic representation of VA-ECMO and VV-ECMO configurations.

In the recent period, due to Covid-19 pandemic, there has been a steady increase in ECMO use [32]. Since covid-19 patients may be affected by acute respiratory distress syndrome (ARDS) refractory to mechanical ventilation and traditional strategies, ECMO represents an alternative method to cure these patients assuring blood oxygenation [33, 34]. At the time of writing this thesis, there were 3684 patients treated with ECMO [35].

1.2.3 Extra corporeal CO_2 Removal - ECCO2R

Extra corporeal carbon dioxide removal (ECCO2R) is a technique that provides artificial respiratory support removing CO_2 from the blood through a membrane oxygenator [36]. ECCO2R devices include a drainage cannula placed in a central vein (VV configuration) or artery (AV configuration), an artificial lung, and a return

cannula into the venous system [37].

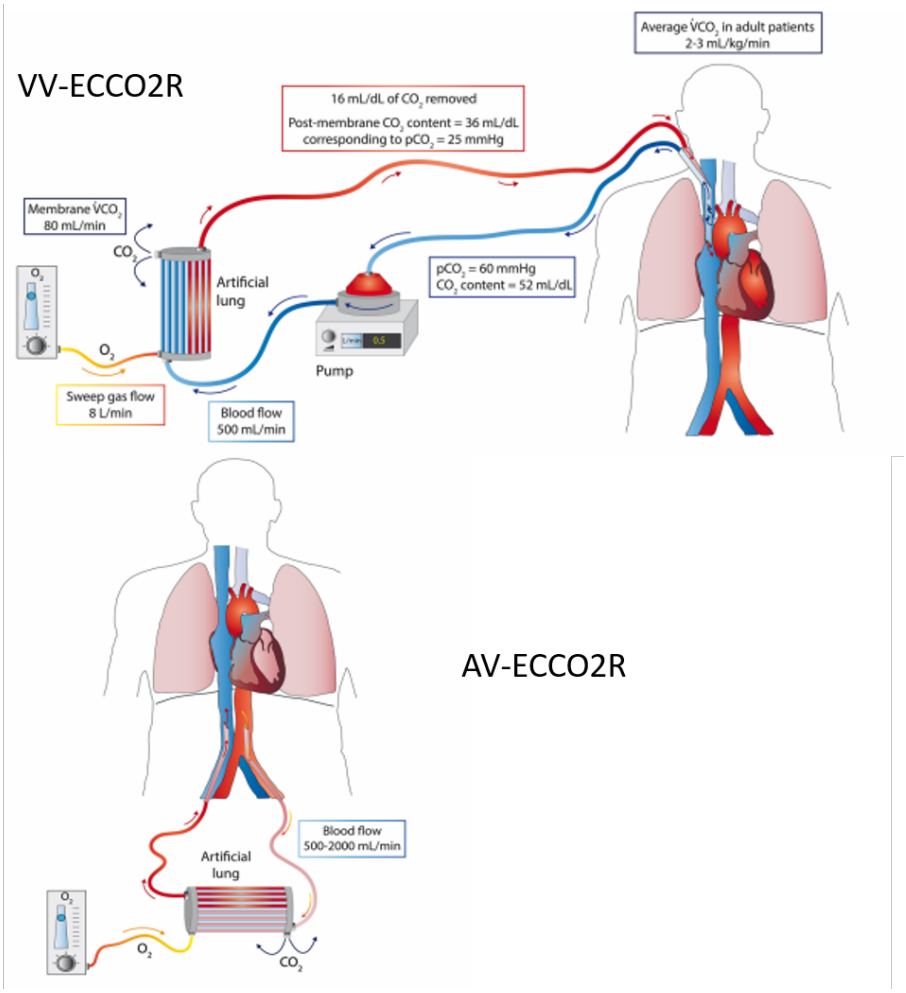

Figure 1.9: Schematic representation of VA-ECCO2R and VV-ECCO2R configurations.

Application of high sweep fresh gas flow generates a diffusion gradient which allows CO_2 removal [38]. Moreover, CO_2 removal rate depends on the blood flow to the membrane: 1 L of blood contains around 500 mL of CO_2 or more and the CO_2 production per minute is about 200–250 mL/min; thus a blood flow of 0.5 L/min would be sufficient to remove all of the CO_2 produced by the body [39]. Therefore, meaningful CO_2 removal rate can be obtained with a blood flow of 300-1000 ml/min. Although it has been reported that a blood flow of 300–500 mL/min potentially replaces about 50% or more of the exchange function of the native lung [39, 40], the percentage is very often lower, as it depends on the actual blood CO_2 content, haemoglobin concentration and the exchange performance of the membrane. There-

fore, ECCO2R may typically remove about 25% of total CO_2 production [39, 40] Since ECCO2R is a low blood flow procedure, roller pumps can be used even though this kind of procedure can last for days [41]. Further, as reported in Figure 1.9, AV configuration, is pumpless. Considering the low blood volume involved, blood is pushed through the oxygenator by patient's arterial pressure in this configuration. ECCO2R is applied to treat hypercapnia condition, that is a condition of abnormally elevated carbon dioxide levels in the blood. Hypercapnia can be generated by pathophysiological changes in the respiratory system or from specific mechanical ventilation protective strategies [42]. Hypercapnia negatively affects several extrapulmonary organs, in particular brain and cardiovascular system. By increasing cerebral blood flow, hypercapnia elevates intracranial pressure [42, 43]. Hypercapnic acidosis increases pulmonary vasoconstriction and, in addition to microvascular alterations and the effects of positive-pressure MV dramatically increases right ventricular (RV) afterload [44]. At the same time, hypercapnia and hypercapnic acidosis decrease myocardial contractility. This altered hemodynamic profile contributes to RV-arterial decoupling and acute RV dysfunction [42, 44]. ECCO2R is used to treat ARDS patients and treat severe asthma, chronic obstructive pulmonary disease (COPD) and as bridge to transplantation strategy. ARDS patients are commonly treated with invasive mechanical ventilation. However, mechanical ventilation carries the risk of ventilator-induced lung injury (VILI), due to inhomogeneous lung overdistention. In order to reduce VILI occurrence, driving parameters of the mechanical ventilator can be reduced (protective ventilation). However, this strategy may lead to hypercapnia condition. ECCO2R can be used to remove the excess of CO_2 from patient's blood, and allow protective ventilation, thus reducing VILI. Further, the use of ECCO2R has been associated with facilitation of weaning from invasive mechanical ventilation (IMV), and also with support to non-invasive ventilation (NIV), avoiding intubation of the patient. Finally, since ECCO2R prevents the use of IMV in favour of NIV, it can be considered a bridge to lung transplant procedure, since it limits the adverse effect of IMV that can preclude lung transplantation.

1.3 Oxygenator exhaust capnometry

All the ECLS procedures mentioned in the previous sections represent complex systems that require strict monitoring of both patient and device conditions. As previously mentioned, all ECLS procedure involves a membrane oxygenator, that is responsible for blood oxygenation and carbon dioxide removal from patient's blood. Removed carbon dioxide is released in the environment as exhaust gas, through the gas outlet connector of the MO. Therefore, the measurement of CO_2 removed by the MO can be achieved by placing a CO_2 sensor (also called capnometer) at the MO exhaust port. This method is called "oxygenator exhaust capnometry". In this section, the importance of CO_2 concentration measurement in the oxygenator exhaust gas is disclosed. CO_2 removal monitoring during cardiopulmonary by-pass is considered a recommended guideline for practice by the American Society of Extra Corporeal Technology [45]. Carbon dioxide tension (PCO_2) measured by exhaust oxygenator capnometry is representative of the interaction of CO_2 production and its elimination by the artificial lung. Therefore, this measurement can provide important information related to both efficacies of CO_2 removal and metabolic status of the peripheral organs and the adequacy of their perfusion [46]. From the measurement of CO_2 concentration of exhaust gas is possible to obtain the carbon dioxide removal rate through the following equation:

$$VCO_2(ml/min) = \frac{GF(ml/min) \cdot ePCO_2(mmHg)}{760(mmHg)} \tag{1.2}$$

where: VCO_2 is the CO_2 removal rate expressed in mL/min, $ePCO_2$ is the carbon dioxide concentration in the exhaust gas expressed in mmHg and GF is the sweep gas flow provided to the oxygenator expressed in mL/min. During CPB, an alternative method to estimate VCO_2 is based on Fick's principle, and does not require knowing the $ePCO_2$ value:

$$VCO_2 = Q_c \cdot (\text{mixed venous } CO_2 \text{ content - arterial } CO_2 \text{ content}) \tag{1.3}$$

Venous and arterial CO_2 content can be acquired by blood gas analysis or in-line blood parameters monitoring devices. However, even though Fick's law is accurate for determination of VO_2, for carbon dioxide is less precise, since CO_2 in the blood

is carried by different ways: dissolved (about 10 %), in form of bicarbonate (about 10 %) and associated with proteins (about 10 %) [47]. Experimental studies have demonstrated that VCO_2 value obtained through exhaust oxygenator capnometry (Equation 1.2) is more reliable than VCO_2 obtained through blood gas analysis (Equation 1.3) [48, 49]. Even though in-line blood monitoring systems (e.g. Terumo CDI 500) have been demonstrated to be reliable in measuring PCO_2 value [50], they present several disadvantages when compared to gas-phase monitoring methods such as oxygenator exhaust capnometry [51]. First, in-line blood measurement has lower long-term stability, and calibration with a gas sample is always required before use to not affect measurement accuracy. Further, since the in-line blood measurement exploits fluorescence, dedicated disposable microsensors are needed, increasing the complexity and cost of the disposable circuit, which are also characterized by lower durability. Finally, while gas-phase measurements are non-invasive, in-line blood measuring systems involve blood contact and by-pass line, with the consequent risk of blood coagulation and air infusion.

Oxygenator exhaust capnometry can be used to estimate arterial carbon dioxide tension ($PaCO_2$) during CPB. Several works have demonstrated a good correlation between $ePCO_2$ and $PaCO_2$ during CPB procedures [52, 53, 54]. Further, VCO_2 is considered a good predictor of anaerobic metabolism during CPB that leads to an increased CO_2 production by the patient's metabolism [55], and also its monitoring is important to prevent postoperative renal insufficiency[49, 56]. Finally, since during CPB CO_2 is provided to the patient to facilitate the air removal from cardiac cavities and improve neurological outcome, a massive quantity of carbon dioxide will enter the systemic circulation hypercapnia condition. Oxygenator exhaust capnometry can be used to monitor the non-metabolic CO_2 and allow its removal increasing the sweep gas flow [49]. Monitoring of CO_2 in the oxygenator exhaust gas is also important to evaluate the membrane oxygenator's performance. Since MO failure is the second most common mechanical complication during ECLS, its monitoring is crucial in order to recognise the right timing for ML replacement [29]. Causes of MO failure include either fibrin clot formation or water condensation, both of which diminish the membrane's ability to transfer oxygen and CO_2. An incidence

of oxygenator failure or clot in the oxygenator is reported in 21.6% of respiratory ECMO runs in the neonatal and pediatric population [57]. Continuous monitoring of CO_2 concentration in the oxygenator exhaust allows calculation of the so-called "membrane oxygenator dead space" (VDsMO), that represent the number of fibres within the oxygenator that are ventilated but not perfused due to clot formation or water condensation on fibres, and therefore does not participate to gas exchange [58]. Considering the parallelism between the artificial lung and natural lungs, VDsMO can be calculated similarly to the respiratory dead space, that is obtained using the Bohr equation:

$$V_{\mathrm{D}} = \frac{PaCO_2 - PeCO_2}{PaCO_2} \cdot V_{\mathrm{T}} \tag{1.4}$$

where: V_D is the respiratory dead space, $PaCO_2$ is the partial pressure of carbon dioxide in the arterial blood [mmHg] and $PeCO_2$ is the partial pressure of carbon dioxide in the expired air [mmHg]. Similarly, for the membrane oxygenator, the dead space can be calculated as follow:

$$VDsMO[\%] = \frac{PCO_2out - ePCO_2}{PCO_2out} \cdot 100 \tag{1.5}$$

where: *VDsMO[%]* is the MO dead space expressed as percentage, PCO_2out is the carbon dioxide in the blood downstream the oxygenator [mmHg] and $ePCO_2$ is the carbon dioxide concentration measured in the oxygenator exhaust [mmHg]. PCO_2out can be obtained through BGA or in-line blood monitoring device. In case of MO failure, $ePCO_2$ will drop while PCO_2out will increase , leading to an higher VDsMO meaning that the gas exchange is impaired. On the other hand, if the CO_2 produced by the patient metabolism decreases, the difference between PCO_2out and $ePCO_2$ will remain constant. Therefore, it is possible discriminate between $ePCO_2$ reduction due to MO failure or $ePCO_2$ reduction due to change in patient's conditions. This kind of monitoring of the VDsMO allows to promptly detect the decrease in MO performance, and eventually prepare the MO substitution in advance.

During ECMO procedure, monitoring MO performance may provide information regarding both the patient's lung status and the MO contribution to the global ventilation, therefore guiding the weaning process [59]. In $ECCO_2R$, the measure-

ment of CO_2 concentration in the exhaust gas and of CO_2 removal rate represents a key parameter to estimate the treatment progress, and evaluate the performance of ECCO_2R membrane in terms of CO_2 clearance.

In conclusion, oxygenator exhaust capnometry can be considered a useful tool for monitoring both the patient's status during the ECLS procedure and allowing correct management of the procedure and improving its safety, assuring a better patient outcome.

Despite its relative ease, oxygenator exhaust capnometry is not routinely applied, as some practical issues remain unsolved in providing a reliable measurement of CO_2 removal from the patient. Usually, oxygenator exhaust capnometry is performed using CO_2 sensors intended for respiratory monitoring, placing the sensor at the gas outlet connector of the MO once per day [58], and obtaining the relevant information from the CO_2 concentration value. However, this kind of measurement does not allow to fully exploit the oxygenator exhaust capnometry potential. Only two devices intended for oxygenator exhaust capnometry are available on the market, the Hemolung RAS (A-Lung Technologies, Inc.) that is a device for ECCO2R procedure with a built-in CO_2 sensor that allows measurement of extracted CO_2, and System M4 (Spectrum Medical Ltd.) a multi-parameter monitoring system intended for ECLS procedures. In the next chapter, CO_2 measuring principle and state of the art of CO_2 sensors are disclosed, as well as the requirements that a CO_2 sensors intended for ECLS applications should meet.

Chapter 2

CO_2 Concentration Measurement

In this section, the measuring principle used for measurement of CO_2 is described, as well as methods to implement it. State-of-the-art sensor architecture used in carbon dioxide measurement in medical applications are also disclosed. Finally, an analysis of the requirements that should be met in the design of a CO_2 sensor intended for ECLS application is reported.

2.1 CO_2 concentration measuring principle

Even though there are several methods that can be used for CO_2 measurement, based for example on chemical or photoacustic principles, optical-based sensors represent the state-of-the-art in the measurement of CO_2 concentration in gases [60]. The potential of optical methods of gas analysis exceeds that of electrochemical and catalytic methods, ensuring high speed, selectivity, stability to aggressive media and long service life. These are typically based on infrared spectroscopy, a well-known technique that exploits molecules' ability to absorb light at specific wavelengths related to vibration and rotation mechanisms of molecules [61]. The Bourger–Lambert–Beer Law describes the working principle of these sensors [62]:

$$dI = -\alpha(\lambda)cI_o dx \tag{2.1}$$

where I is the transmitted radiation intensity, Io is the incident radiation intensity, c is the analyte concentration, $\alpha(\lambda)$ is the analyte-specific absorption coefficient, and x

represent the optical path length. The integral form of the Bourger–Lambert–Beer's Law,

$$I = I_o e^{-\alpha(\lambda)cx} \tag{2.2}$$

shows that it is possible to calculate the analyte concentration observing variation of the transmitted radiation I [arbitrary unit], as it represents attenuation of the incident radiation Io [arbitrary unit] once it has passed through the optical path x [cm] containing an amount c [mol/l] of the analyte with absorption coefficient $\alpha(\lambda)$ [$\mathrm{l \cdot mol^{-1} \cdot cm^{-1}}$]. In Equation 2.2 is highlighted that the absorption coefficient is a wavelength-dependent parameter, so to correctly exploit the absorption measurement principle is of paramount importance that the incident light has a spectrum that includes the absorption band of the analyte of interest. For CO_2, the incident light spectrum shall be in the mid-infrared (mid-IR) region (3 - 8 μm) as the principal absorption peak for carbon dioxide is located at 4.25 μm [63]. Further, to obtain a direct measurement of the analyte of interest and avoid cross-response to other chemical species, no other compounds shall have absorption bands included on the incident light spectrum. Therefore, the whole composition of the oxygenator exhaust gas mixture must be considered to develop an efficient CO_2 sensor for ECLS applications. The exhaust gas of a membrane oxygenator during ECLS procedure contains a variable concentration of the following chemical species: Oxygen (O_2), Nitrogen (N_2), Carbon Dioxide (CO_2), and water vapour. As infrared radiations are absorbed only by asymmetrical molecules, only CO_2 and water vapour (H_2O) have absorption bands in the mid-IR region. Absorption spectra of CO_2 and H_2O obtained from the HITRAN database [64] are reported in Figure 2.1.

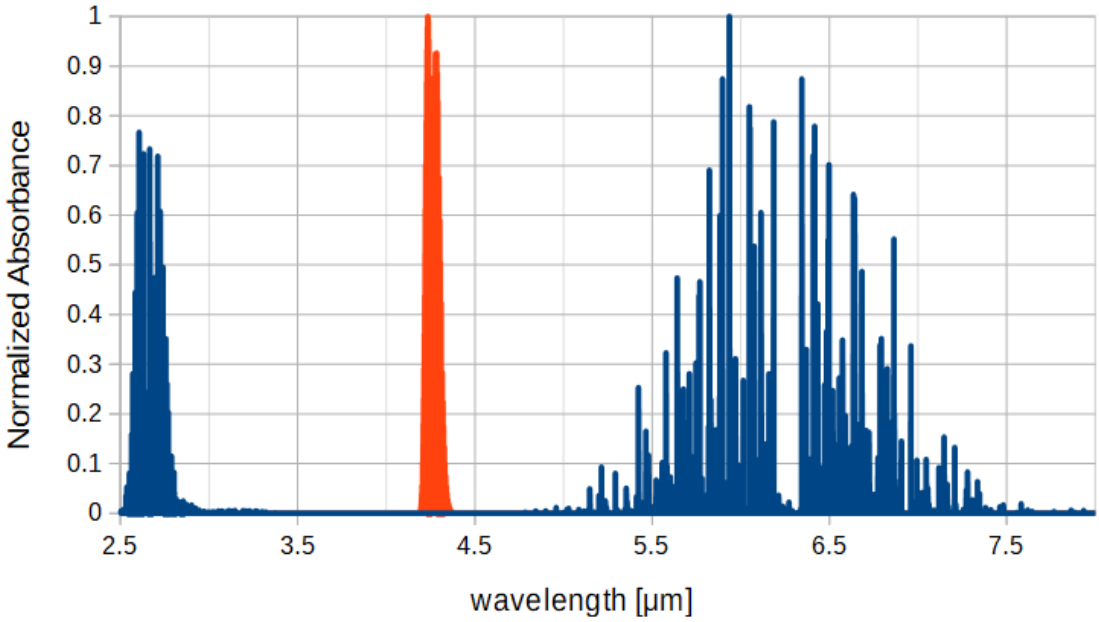

Figure 2.1: Absorption bands of CO_2 (orange) and H_2O (blue).

Method to obtain emission in the mid-IR spectrum used in the currently available capnometers are based on Nondispersive infrared (NDIR) technology since no dispersive elements (e.g. prism) are used to separate the emitted broadband radiation into narrow spectrum suitable for analyte sensing. Typically, the emitted radiation is generated by a broadband emitting incandescence light source. The spectral emission characteristic of an incandescent light source can nearly be described by the Planck's law for black body radiation. The emitted light intensity and the spectral distribution is only depending on the surface temperature of the emitter element [65]. To prevent cross-response from compounds other than the one of interest, the broadband emission spectra generated by the incandescent light source is filtered by optical bandpass filters. Coupling a broadband emitting incandescence light source with at least two optical filters, one for the analyte of interest absorption and one for reference, a differential measurement can be made and interfering broadband absorption is prevented. Different optical set-ups are implemented in CO_2 sensors used in capnometry:

- Emission light spectrum is generated through an incandescent filament. The broadband spectrum is directed to a single IR detector. The emitted light is

filtered and modulated by a rotating wheel placed in the optical path [66].

- The emitted light is directed through the measuring chamber to a spectrally separating beam splitter that directs the light towards two differents IR detectors [67, 65].

- The emitted IR radiation reaches two different detectors that have a specific IR bandpass through different optical paths [68].

Usually, detector elements are thermophiles or pyroelectric detectors.

An alternative optical set-up for CO_2 measurement in gas consists of the use of a narrow spectrum emitting diode coupled with an appropriate photodetector. This solution is possible thanks to the use of light-emitting diode (LED) and photodetector (PD) realized with Indium (In), Arsenic (As), Antimony (Sb) epitaxial layer on Indium (In) Arsenic (As) substrate (InAsSb/InAs optical element) [69]. Using appropriate mid-IR LED and PD an optopair, i.e., a source and detector elements that are optically and spectrally matched, CO_2 measurement can be made. Optical coupling of InAsSb/InAs LED and PD allows the emission and detection of IR radiation near 4.2 μm that comprises the principal CO_2 absorption peak. Further, the narrow emission and detection spectra that characterize InAsSB/InAs optical elements allow the direct measurement of CO_2 even in the presence of water vapour, as reported in Figure 2.2.

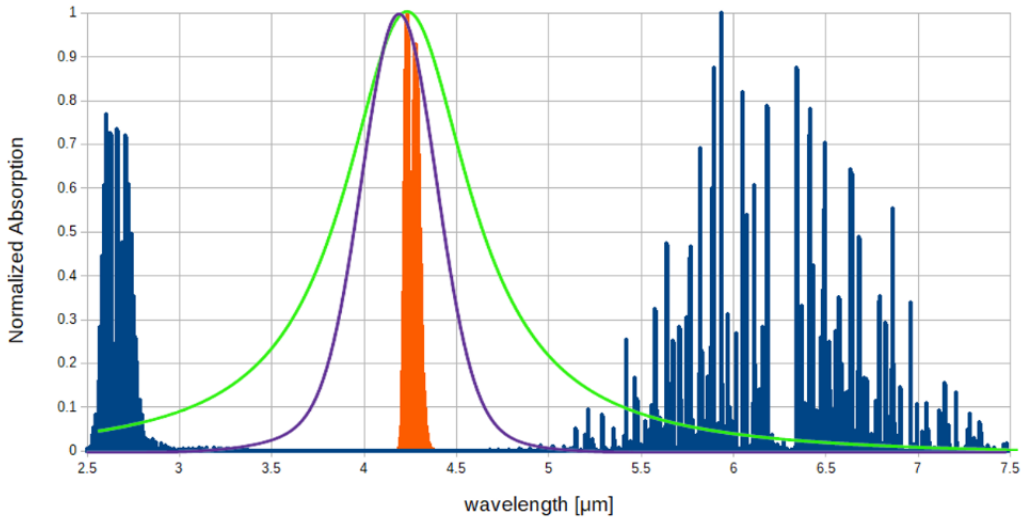

Figure 2.2: InAsSb/InAs LED (green) and PD (purple) spectra. Absorption bands of CO_2 (orange) and H_2O (blue).

Therefore, an optical set-up that involves InAsSb/InAS optopair allows the design of an optical sensor without using mechanical modulators or interference filters, thus allowing a simpler optical design of the sensor, involving fewer components. In the following figure is reported the schematic of a single channel architecture, meaning that the optopairs is made up by a single LED and a single PD.

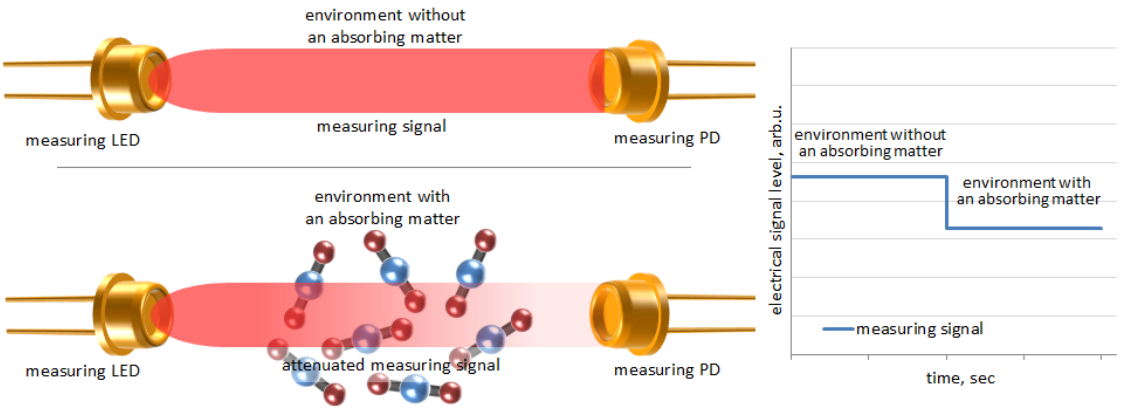

Figure 2.3: Schematic representation of a single channel optopair architecture

2.2 State-of-the-art CO_2 sensor architectures

In commercially available capnometers for respiratory monitoring, two different sensor's architectures are used for measurement of CO_2 concentration [70]:

- non-diverting (Main-stream);
- diverting (Side-stream).

In non-diverting, or Main-stream, capnometers architecture, the optical absorption measurement is taken in-line with the respiratory stream, through a measuring cuvette transparent to the mid-IR radiation. The acquired data are then sent from the optical sensor probe to a display unit. In Side-stream architecture, a portion of the gas is pulled from the respiratory stream flow into the absorption chamber, that is spatially separated from the main respiratory flow. The optical sensor is contained within the control unit that display the CO_2 concentration value [65, 71, 72]. Figure 2.4 shows a schematic representation of Main-stream and Side-stream sensors architecture.

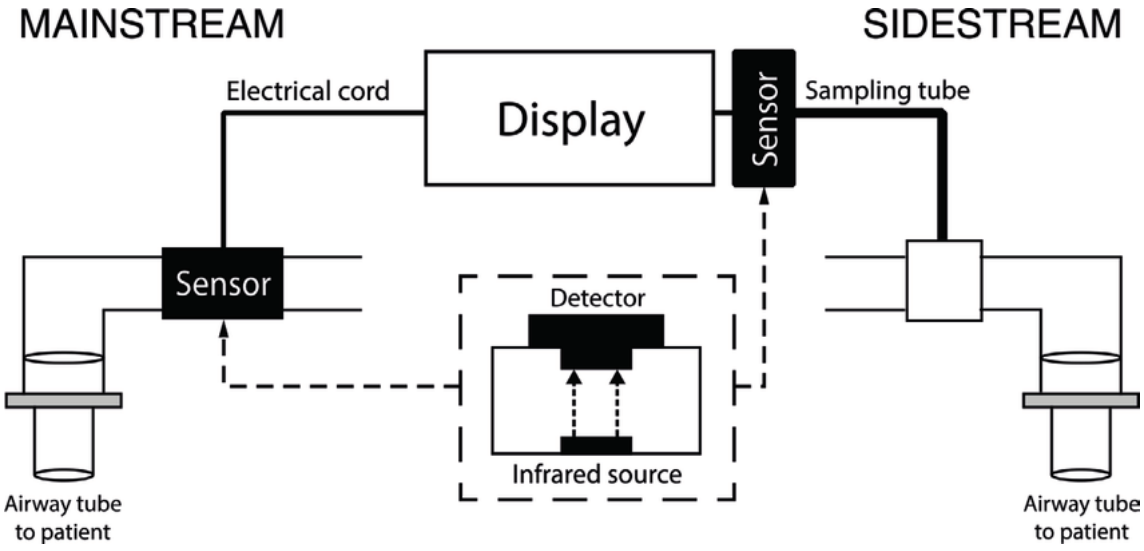

Figure 2.4: Main-stream and Side-stream capnometry architecture

In main-stream capnometers, the measuring cuvette shall be designed to allow the mid-IR beam generated by the emitter source to reach the detector crossing the gas to be measured. In order to achieve transparency to mid-IR beam, cuvette used in main-stream capnometry are designed with two optical windows, typically made

of sapphire glass. Exhaled breath contains water vapour, that is able to absorb mid-IR radiation. However, CO_2 absorption band at 4.25 μm is relatively free water vapour interference. However, water vapour may represent a problem since it can condensate on the optical windows and lead to incorrect CO_2 concentration readings. This effect has been effectively minimized in main-stream systems by heating the airway adapter, and its windows above body temperature [71]. In side-stream systems, the sampled gas temperature decreases toward room temperature during its transit from the patient connection to the sensor unit [73]. Consequently, condensation on the sampling tube walls happens, resulting in a decrease in the partial pressure of water vapour from the Body Temperature and Pressure Saturated condition (BTPS) value of 47 mm Hg to much lower values. This decrease in water vapour pressure can cause an apparent increase in CO_2 concentration [74]. Side-stream devices compensate by software water vapour removal, and as a result, may introduce errors since assumed conditions may be very different from actual, and physical conditions may change over time. Main-stream CO_2 correctly read the partial pressure of CO_2 at the conditions in the breathing circuit typically at or near BTPS and do not require software compensation for water vapour [71]. Further, in side-stream sensor water vapour condensation or water-like substances (generated by patient's secretions) may lead to partial obstruction of the sampling line and, therefore, increase the tube's resistance, affecting the CO_2 measurement. In the most severe cases, the sampling tube may be totally occluded, preventing the gas from reaching the sensor unit.

2.3 Design Requirements analysis for ECLS CO_2 sensor development

In this section, the requirements that should be met in the design of a CO_2 sensor intended for ECLS application are analyzed and disclosed. The following aspect should be considered:

- sensor accuracy

- water vapour condensation
- sensor architecture
- gas flow measurement
- interface to other devices

Since there are no standards that specify the minimum accuracy level for a CO_2 sensor intended for ECLS application, the "closest" applicable standard is ISO 80601-2-55 - Medical electrical equipment — Part 2-55: Particular requirements for the basic safety and essential performance of respiratory gas monitors, that specifies particular requirements for the basic safety and essential performance of a respiratory gas monitor. Clause 201.12.1.101 of the ISO 80601-2-55 specifies the minimum accuracy level for different gas concentration measurement. For carbon dioxide, minimum accuracy level specified by the standard is [75]:

$$CO_2\ Measurement\ Accuracy = \pm 0,43\% + 8\%\ GAS\ LEVEL \tag{2.3}$$

where *GAS LEVEL* is the gas concentration expressed in volume percentage. However, CO_2 sensors used for respiratory monitoring, shown better accuracy performance than the one reported in the standard. For example, Medtronic Microstream CO_2 sensor, used in side-stream capnometers, has an accuracy of ± 2mmHg for carbon dioxide concentration between 0-38 mmHg, and ± 5% of reading + 0.08 for every 1 mmHg above 38 mmHg [76]. An mmHg is equal to a concentration 0,13% in volume percentage. Respironics Capnostat 5, is a main-stream capnometer and show the following accuracy performance: ± 2mmHg in the range 0-40 mmHg, ± 5% of reading in the range 41-70 mmHg, ± 8% of reading in the range 71-100 mmHg and ± 10% of reading in the range 101-150 mmHg [77]. A CO_2 sensor designed for ECLS application should have similar accuracy performance, or at least within the accuracy limits specified by the ISO 80601-2-55 standard.

A second aspect to take into account is that in ECLS procedures water vapour condensation at the exhaust port of the MO occurs. Due to the microporous nature of the membrane, blood plasma can evaporate at the liquid-membrane interface and diffuse as water vapour across the pores into the fibres' intraluminal space, in which

sweep gas flows. Water vapour condensation at oxygenator gas outlet connector is associated with the sudden cooling of the gas flow in the proximity of the outlet cover, where the warming effect of blood is no longer present. Since condensation within the fibres of the membrane oxygenator can reduce the gas transfer efficiency, several methods have been proposed to prevent the condensation effect, such as warming the gas at the inflow or outflow section, creating a warm environment around the whole oxygenator, or blowing off the condensate from the clogged fibres by gas flushing. Further, it is noteworthy that the effect of water vapour condensation is worse in ECLS procedures than in exhaled breath monitoring, due to the presence of a continuous gas flow and higher flow rate at the oxygenator exhaust port. Therefore, in the design of a capnometer for ECLS application, water vapour condensation shall be considered and method to avoid it implemented since it can affect the CO_2 concentration measurement based on optical methods. Considerations about the architecture to implement (main-stream or side-stream) are important in designing a CO_2 intended to be connected to the oxygenator exhaust connector. Main-stream architecture has the advantage that no sampling line is needed and therefore, there is no risk of obstruction. Further, water vapour condensation can be avoided heating the sensor [78], and it is not affected by changes in water vapour pressure [49]. One of the main disadvantages is the difficulty of connecting the cuvette of a main-stream capnometer to the standard size (diameter of 1/4" or 3/8") exhaust connector of a membrane oxygenator. Therefore a method that allows an easy connection to the oxygenator should be considered. In side-stream sensor the water vapour can easily condensate in the tube used to bring the gas sample to the measuring chamber, leading to clotting of the sample line and compromising the correct measurement [71]. Further, the use of Side-stream CO_2 sensor at the oxygenator exhaust port has the drawback of the environmental air pulled to the measuring chamber together with the exhaust gas, which leads to the incorrect estimation of CO_2 removed from the patient [79]. This can happen especially if the sampling flow rate of the side-stream sensor is equal or higher than the exhaust gas flow rate. Considering that during the ECLS procedure, the sweep gas flow can be changed often, the risk of acquiring environmental air, especially during pediatric

procedures that involve lower sweep gas flow is high. Position of the sampling line is important, most of MO has one ore more vent ports used for protection against blockage of the exhaust gas line, that can lead to increased pressure, and transfer of microemboli to the blood [80]. If the sampling line is placed too close to a vent port, the sample can be diluted with environmental air. To improve side-stream sensor accuracy during ECLS procedures, the sampling tube may be placed inside the MO exhaust port. [81]. In this, way the gas sample is gathered directly from the gas compartment of the MO, preventing its dilution with environmental air. However, this solution brings to sterilization issues that are not compatible with clinical routine in the intensive care unit (ICU). Therefore, in ECLS applications, a Main-stream CO_2 sensor seems more appropriate than a Side-stream sensor. In order to allow measurement of VCO_2 as reported in equation 1.2, a method to acquire the gas flow applied to the oxygenator shall be implemented. Regarding time resolution of the CO_2 concentration measurement, differently from respiratory capnometry in which high time resolution is necessary to obtain information on the end-tidal CO_2, respiratory rate and exhaled breath waveform, capnometry applied to ECLS procedures does not require such highly time-resolved measurement, as in ECLS applications the oxygenator exhaust gas flow and CO_2 concentration change slowly. Therefore, temporal resolution of the order of minutes is sufficient to extract information about the ECLS procedure, since are used for evaluation of long-term therapy progress and trends. Finally, a CO_2 sensor for ECLS application should not be designed as a standalone device, but rather it should be interfaced with monitoring devices already used to monitor the patient's condition or to the ECLS device itself.

Chapter 3

Sensor Development

In this section, the development of the CO_2 sensor is described. At first, the flow measurement section's development is disclosed, and then the sensor's section for carbon dioxide concentration monitoring is described. Temperature effect on optical elements performance is analyzed both theoretically and experimentally, and a method for compensation of the temperature effect is proposed.

3.1 Gas Flow measuring section

As reported in Equation 1.2, to measure VCO_2, information on gas flow is necessary. Mass gas flow sensors represent the state of the art technology for gas flow measurement. These sensors are based on the thermal measurement principle. Within the sensors, MEMS-based calorimetric microsensors measure the changes in temperature gradient caused by mass flow. Figure 3.1 shows the measuring principle exploited by these sensors.

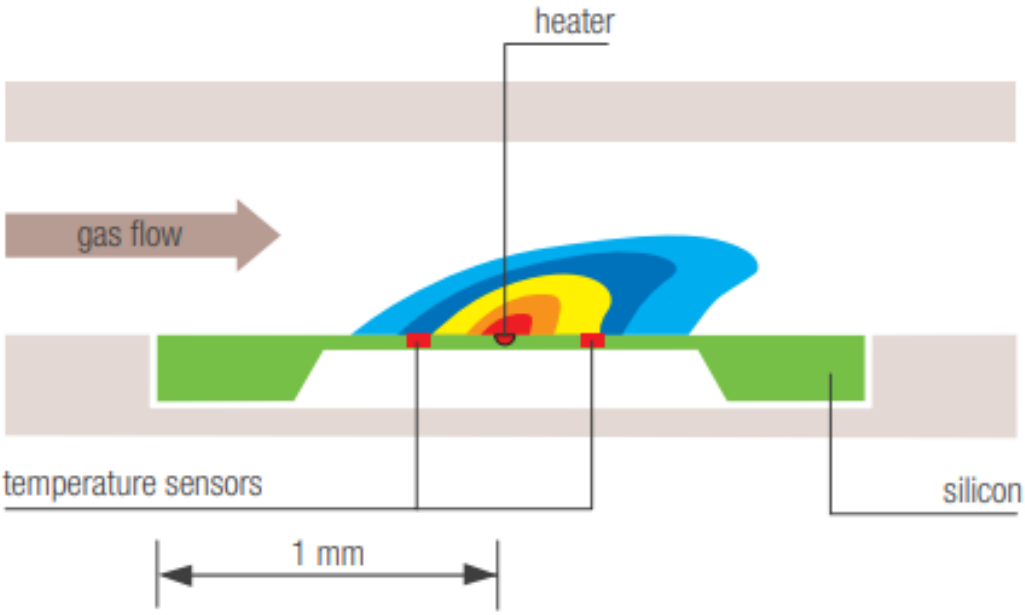

Figure 3.1: Mass flow sensor measuring principle.

For the development of the gas measuring unit, we focused on two mass airflow sensor: Sensirion SFM4100 and Posifa PMF4000. According to their datasheets, both sensors have a measurement range of 0-20 SLM (Standard Liter per Minute) and similar accuracy performance. Sensors performance has been tested comparing their output to a reference flow sensor, at several flow rate values. From the experimental evaluation, both sensors outputs are close to the flow rate measured with the reference instrument, however, SFM4100 shows slightly better performance with an average error of 0,12 SLM against the average error of 0,18 SLM of PFM4000. Considering the final application, the presence of water vapour within the gas exhaust shall be taken into account. If the flow sensor is placed at the oxygenator exhaust port of the MO, water vapour can easily condensate within the sensor leading to incorrect flow rate measurement or sensor failure. Increment of the sensor temperature to avoid the water vapour condensation is not a suitable solution, as it would interfere with the measurement principle exploited by the flow sensor, that depends on the cooling effect applied by a gas flow on a heating element placed within the sensor [82]. Therefore, to avoid measurement error due to water vapour, the GF

measurement section has been designed to be positioned at the inlet port of the MO. Further, positioning of the flow sensor at the inlet gas line of the membrane oxygenator provides the operator direct feedback about the sweep gas flow used for the extra corporeal procedure and can be used to detect the disconnection of the gas line. Considering the positioning at the inlet gas line of the MO, the SFM4100 has the advantage that its connector can be easily substituted and replaced with a connector suitable for the inlet gas tube diameter. For these reasons, we opted for the SFM4100 sensor. The flow sensor data are communicated through I2C interface to the CPU contained in the CO_2 measurement section. In Figure 3.2 is reported the developed sensing platform, made up by two sections, one for measurement of gas flow applied to the MO and one for CO_2 concentration measurement in the exhaust gas.

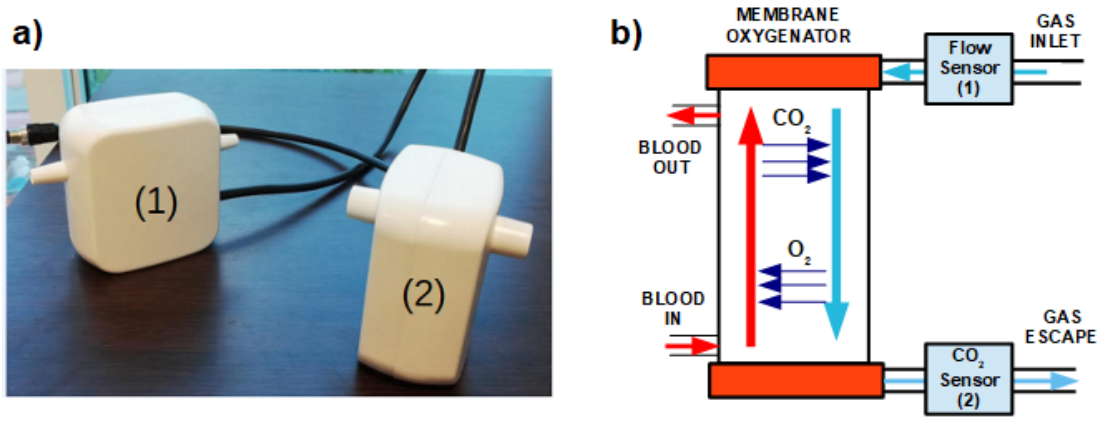

Figure 3.2: (**a**) Developed CO_2 sensing platform. (1) Flow measurement section; (2) CO_2 measurement section. (**b**) Schematic representation of flow sensor and CO_2 sensor on MO.

3.2 CO_2 measuring section

The CO_2 measurement section has been entirely developed and is made up of three subsections:

1. emission stage for the generation of the mid-IR beam;

2. receiver stage for the detection, conditioning and amplification of the optical signal after CO_2 absorption and;

3. CPU for signal acquisition, processing, and communication with the flow sensor section and a host device.

For both emission and detection of the mid-IR beam, optical elements of InAsSb/InAs (LED Microsensor NT, Saint-Petersburg, Russia) are used [83]. LED and PD are placed on opposite sides of a measuring cuvette and are mechanically fixed to assure the correct positioning and optimal optical coupling. In order to improve optical coupling and obtain the best performance in terms of signal-to-noise ratio (SNR), both LED and PD InAnSb/InAs chip are mounted on TO-18 package with a parabolic reflector. The parabolic reflector allows a more directive optical beam to be generated and detected, leading to a higher optical signal acquired by the sensor. Figure 3.3 shows a comparison of beam divergence between optical element with and without the parabolic reflector (data provided by the manufacturer).

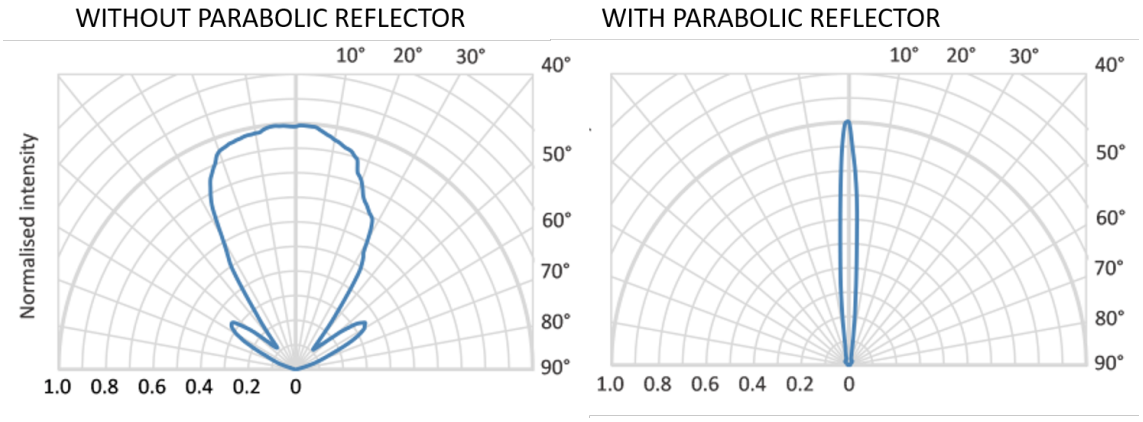

Figure 3.3: Beam divergence comparison between optical element without and with parabolic reflector.

In order to protect the optical elements, a sapphire glass window is mounted on the parabolic reflector. In the following figure, the optical elements package is shown.

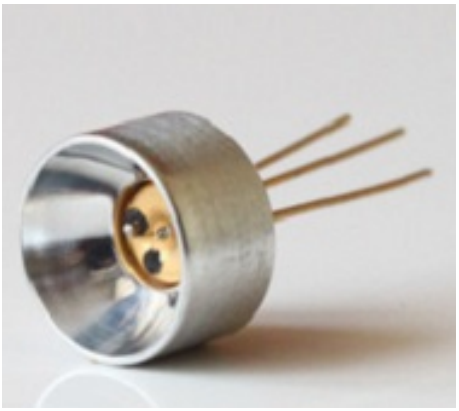

Figure 3.4: InAsSb/InAs optical element package with parabolic reflector.

As only a single LED-PD couple is used, this solution represents a single-channel architecture. Use of the single-channel architecture allows obtaining a simpler device, easy to assemble and cheaper, as no optical filters or beam splitter are used. Since each InAsSb/InAs elements is different in terms of emission efficiency and photosensitivity, the CO_2 sensor hardware has been designed to allow modulation of LED current (through a PWM signal) and setting of receiver stage gain, by the microcontroller unit. This flexibility allows the proper tuning of each optical couple in order to achieve the best performance. As reported in section 2.3, main-stream architecture is considered more suitable for ECLS application than side-stream. Therefore, the CO_2 sensor has been designed following this assumption, and the measuring cuvette designed to be directly connected to the MO exhaust gas connector. In order to prevent water vapour condensation, a heating system has been implemented on both emitter and receiver stage. The Heating system is composed of resistances mounted on the rear of the electronics boards that generate heat, an aluminium ring that surrounds the optical elements and transfers the generated heat along the measuring chamber, and a digital temperature sensor for the temperature monitoring. CPU controls the emitter's temperature and the receiver stages by switching ON and OFF the current circulating in the resistances. A block diagram of the proposed CO_2 sensor architecture is reported in Figure 3.5, while in Figure 3.6 is reported the exploded drawing and a picture of the developed CO_2 sensor.

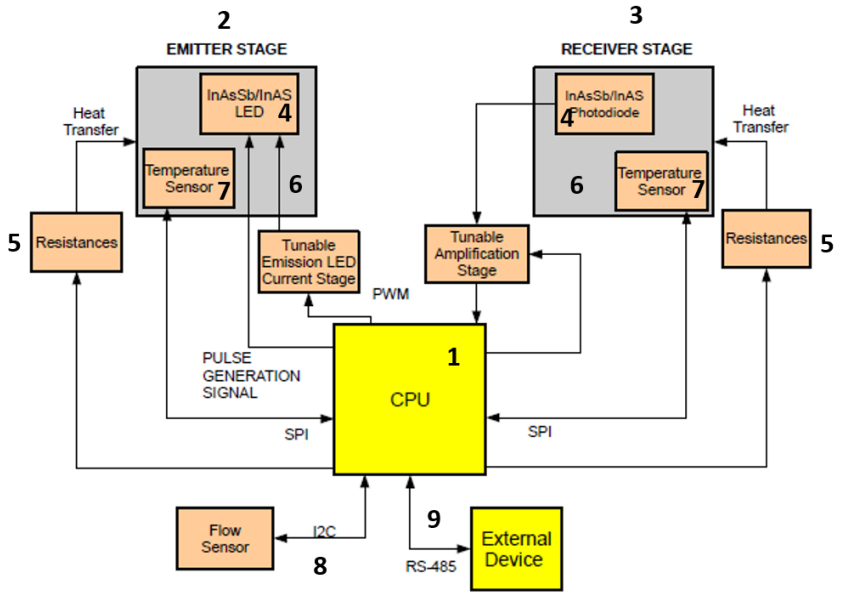

Figure 3.5: Schematic representation of the sensor: (1) CPU board; (2) aluminum rings; (3) emitter board; (4) InAsSb/InAs element; (5) digital temperature sensor; (6) receiver board; (7) heating resistances; (8) Flow sensor communication cable; (9) power supply/RS-485 cable.

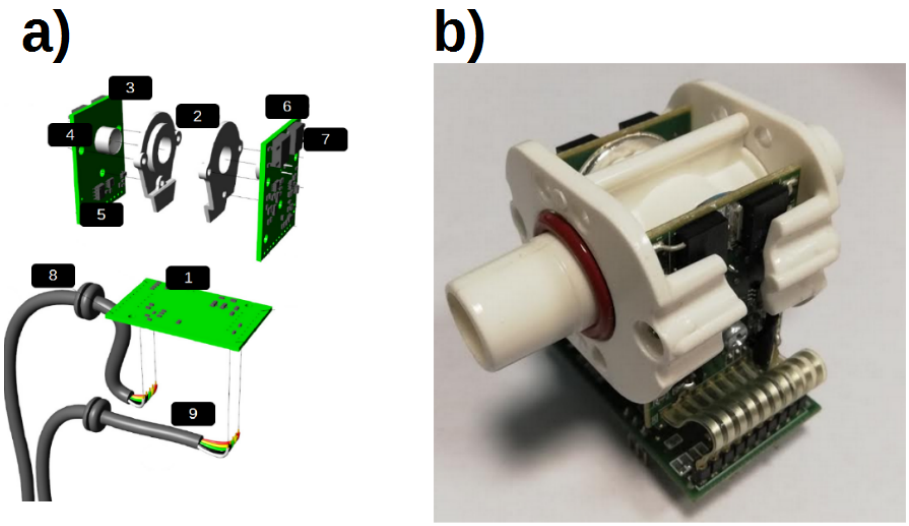

Figure 3.6: (**a**) Exploded drawing of the CO_2 sensor: (1) CPU board; (2) aluminum rings; (3) emitter board; (4) InAsSb/InAs element; (5) digital temperature sensor; (6) receiver board; (7) heating resistances; (8) Flow sensor communication cable; (9) power supply/RS-485 cable. (**b**) Assembly of the developed CO_2 and plastic cuvette.

Thanks to the implemented heating system, the water vapour condensation is prevented not only on optical elements but also in their proximity, obtaining a water-free cuvette. Figure 3.7 shows an example of water vapour condensation on a cuvette placed at MO exhaust port that occurs without implementing a heating system.

Figure 3.7: Effect of water vapour condensation on a test cuvette placed at the exhaust port of a membrane oxygenator.

Further, without implementing the heating system, water vapour condensation leads to total degradation of the optical signal, as confirmed experimentally recording the optical signal from CO_2 sensors without the implemented heating system while relative humidity (RH%) of the gas flow increases. As RH% increases, water vapour starts to condensate on the measuring cuvette walls and optical elements, leading to signal degradation. With the heating system's implementation, the optical signal is not affected by high humidity condition and water vapour condensation, as confirmed experimentally. Figure 3.8 shows the experimental results, comparing the effect of water vapour condensation on the optical signal with and without the heating system's presence.

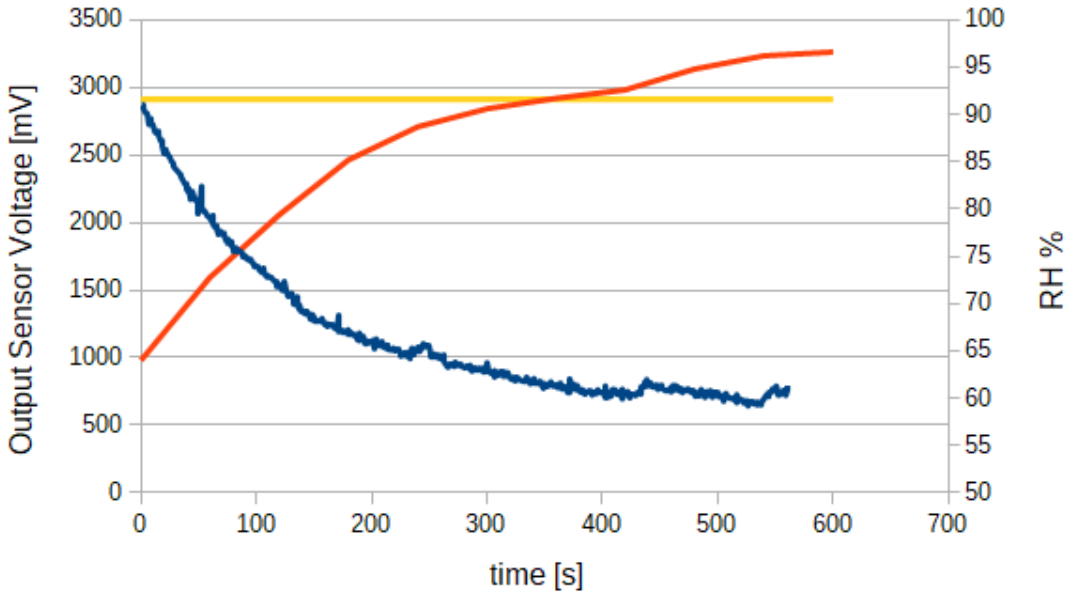

Figure 3.8: Sensor output voltage, without (blue line) and with (yellow line) implementation of the heating system, versus relative humidity (orange line).

The gas temperature at the exhaust port of a MO usually is 38 °C during ECLS procedures such as CPB [84]; therefore, increasing the sensor's temperature measuring chamber to 40 °C prevents water vapour condensation. Even though the sensor's measuring chamber's heating prevents water vapour condensation, an increase in optical elements temperature brings side effects relevant to LED and PD efficiency. Moreover, the implemented heating system's goal is to prevent water vapour condensation not only on optical elements but also on the entire measuring chamber, preventing the formation of water drops that will move on the optical elements over time. For this reason, heating elements larger than the optical elements package has been used. This solution allows a more efficient diffusion of heat along the measuring chamber, preventing the formation of water drops. However, using larger heating elements to improve the heat diffusion leads to larger oscillations in temperature of emitter and receiver stages.

3.3 Temperature Effect on InAsSb/InAs optical elements

Since the temperature affects both InAsSb/InAs LED and PD performance, temperature effect has been analyzed. In this section, both theoretical and experimental analysis of temperature effect on LED and PD are presented. Further, methods to compensate for the temperature effect are disclosed.

3.3.1 Analysis of Temperature Effect on Receiver Stage

The temperature increase of the receiver PD determines an increase of both dark current noise and response time. Dark current noise arises from the generation of a current on a photosensitive device even if photons are not detected. The movement of charges that generates the dark current noise mainly depends on the device's thermal condition, and it increases as the temperature increases. This effect worsens the SNR (signal-to-noise ratio) but can be compensated through post-processing on the acquired signal. Slower PD response can be compensated using an appropriately long duration for emission pulse, being sure that the pulse duration allows the PD to reach the steady-state. In our system, the emission pulses are generated at 100 Hz frequency with a pulse duration of 1 ms. To evaluate if the temperature affects the PD photosensitivity (i.e., the ability of the PD to generate current when hit by photons), a theoretical approach has been used at first. The spectral response of an InAsSb/InAs PD can be described by the sum of two Gaussian curves G1 and G2 [85]:

$$R_{PD}(\lambda, T) = R0 \cdot [K1 \cdot G1(\lambda max(T), \Delta\lambda(T)) + K2 \cdot G2(\lambda max(T) - \lambda_0, \Delta\lambda_0] \quad (3.1)$$

where *R0* is the PD integral photodiode sensitivity [A/W], $\Delta\lambda(T)$ is the FWHM, $\lambda max(T)$ is peak wavelength, *K1*, *K2*, $\lambda 0$ and $\Delta\lambda_0$ are adjustable parameters, set in order to fit the spectral response data provided by the manufacturer at $T = 27$ °C (Figure 3.9). Within the temperature range 0 to 50 °C the following relationships are valid, $\Delta\lambda(T) \sim 0.1\ \lambda max(T)$ and $d\lambda max/dT = 4.5$ nm/°C [85].

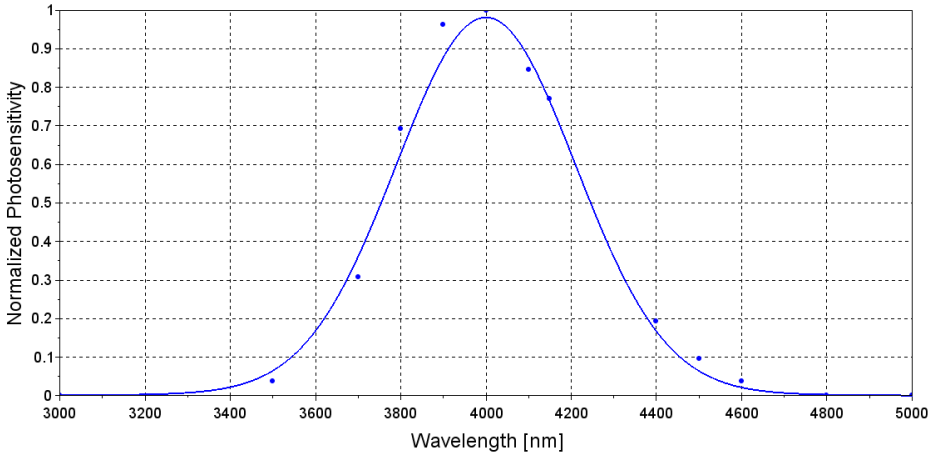

Figure 3.9: Simulated PD spectral response (solid line) and data provided by the manufacturer (dots).

Solving Equation 3.1 for several temperature conditions highlights that temperature variations lead to the shift of the receiver spectrum peak wavelength. At higher temperature, λmax moves to higher values and vice-versa. This effect in shown in Figure 3.10, where detection spectra for several temperature values are reported. From Equation 3.1 is also highlighted that increase on PD temperature only affect photosensitivity in case of large temperature variations, and even in that case photosensitivity variations are small. Therefore the effect on photosensitivity around 40 °C, temperature range at which the heating system works, can be considered negligible.

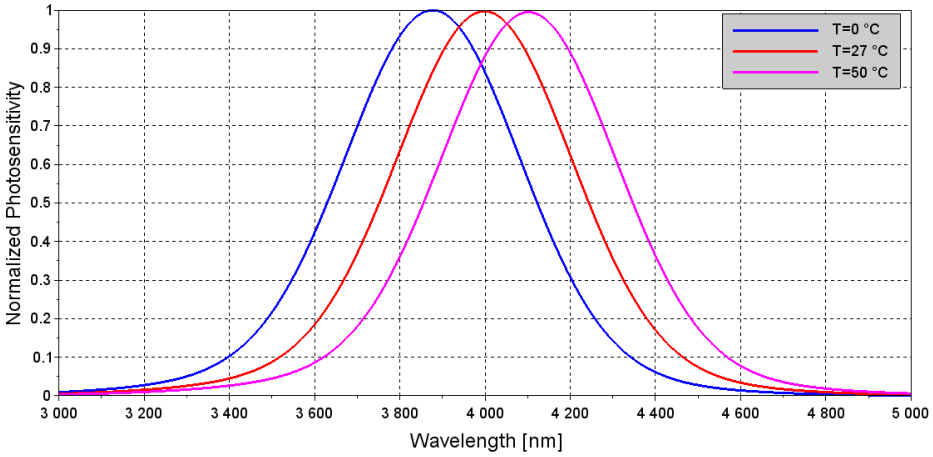

Figure 3.10: Simulation of PD spectra at different temperatures.

3.3.2 Analysis of Temperature Effect on Emitter Stage

Emitted optical power generated by a InAsSb/InAS LED can be described by the following equation:

$$P_{LED}(\lambda, T) = \frac{P0}{\pi} \cdot \frac{\Delta\lambda(T)}{\Delta\lambda(T)^2 + (\lambda - \lambda max(T))^2} \tag{3.2}$$

where $P0$ is the total output power [μW], λ is the wavelength [nm], $\Delta\lambda$ and λmax are the FWHM (Full Width at Half Maximum) and peak wavelength of the emission spectra, respectively. For λmax we considered the value provided by the LED datasheet at 27 °C [83]. As for the PD theoretical description, within the temperature range 0 to 50 °C the following relationships are valid, $\Delta\lambda(T) \sim 0.1$ $\lambda max(T)$ and $\mathrm{d}\lambda max/dT = 4.5$ nm/°C [85]. By solving Equation 3.2 is possible to describe the mid-IR LED emission spectrum at different temperatures as reported in Figure 3.11.

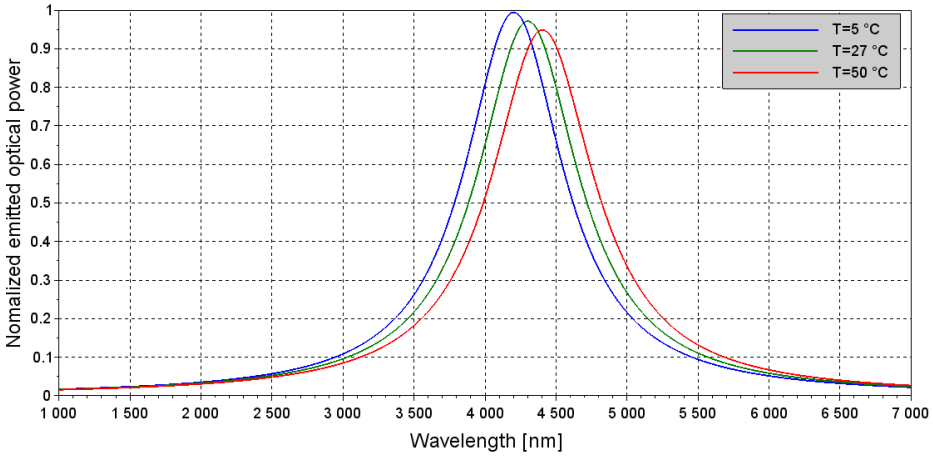

Figure 3.11: Simulation of emission spectra at different temperatures.

As the temperature increases, the peak wavelength of the emission spectrum shifts to higher wavelengths values and at the same time the optical power intensity decreases, as reported in Figure 3.12 where the total output power of the LED was calculated in the temperature range 0-50 °C, integrating the emission spectra through the following equation:

$$P_{LED}(T) = \frac{P0}{\pi} \cdot \int_{\lambda_1}^{\lambda_2} \frac{\Delta\lambda(T)}{\Delta\lambda(T)^2 + (\lambda - \lambda max(T))^2}\, d\lambda \tag{3.3}$$

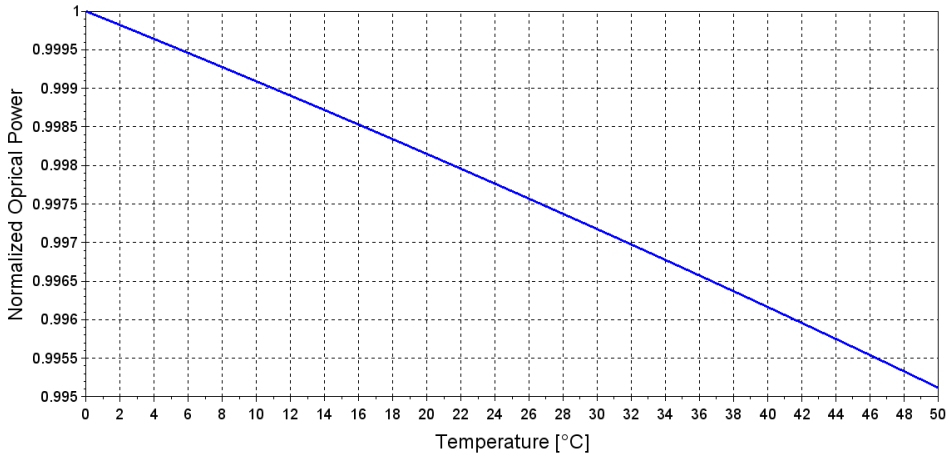

Figure 3.12: Theoretical evaluation of correlation between emitted optical power and temperature.

3.3.3 Experimental Analysis

In order to validate the considerations highlighted through the theoretical analysis of InAsSb/InAs temperature dependency, experimental analysis has been performed. To experimentally evaluate the effect of temperature on the receiver element, the sensor's output signal has been recorded activating the heating system only on the receiver stage to avoid interference due to temperature effect on the emitter element. Therefore, the data collected during the experimental analysis are relevant to the working temperature range of the heating system implemented in the sensor (42-44 °C). The theoretical formulation expressed by Equation 3.1 is confirmed experimentally, as we did not observe any correlation between the receiver stage temperature and the output sensor signal (R^2 = 0,02). The experimental result is reported in Figure 3.13. Therefore, the PD photosensitivity dependency on temperature is negligible in terms of optical signal variation and does not affect the developed sensor's measurement.

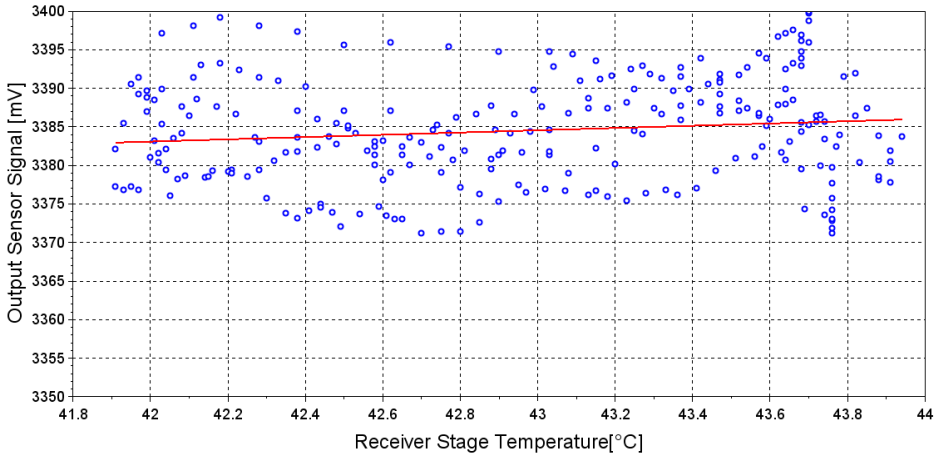

Figure 3.13: Experimental evaluation of correlation between emitted output power and receiver stage temperature. Blue dots represent the sampled value of the output sensor voltage at several temperatures of the receiver stage. Red line represents the linear regression of the data.

Similarly, the temperature effect on the emitter element has been experimentally studied activating the heating system only on the emitter stage, acquiring the sensor output signal at several temperature values of the emitter stage. The experimen-

tal result, reported in Figure 3.14, shows a negative linear correlation with an R^2 coefficient of 0.93.

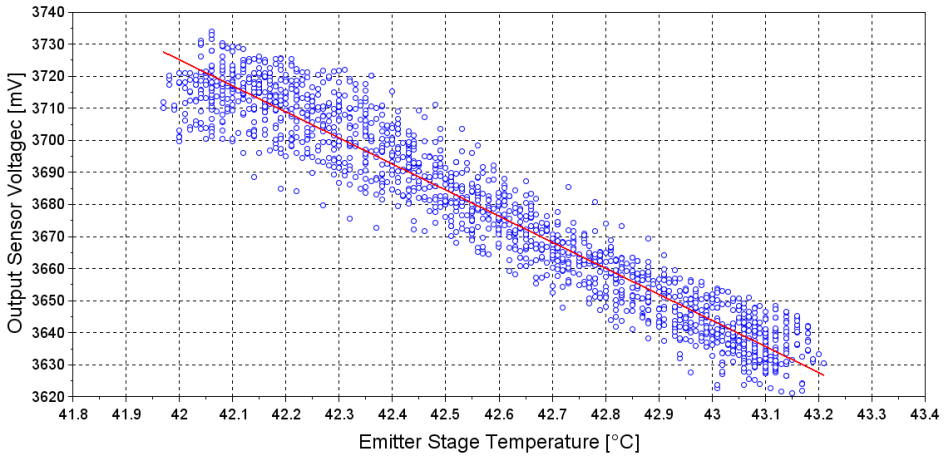

Figure 3.14: Experimental evaluation of correlation between emitted output power and emitter stage temperature. Blue dots represent the sampled value of the output sensor voltage at several temperatures of the emitter stage. Red line represents the linear regression of the data.

However, even though Figures 3.12 and 3.14 both show a negative correlation between emitted optical power and temperature, their slopes are different. In particular, from the theoretical analysis, the sensor signal variation due to the emitter element's temperature variation should be negligible, but this is not confirmed experimentally. Reason for the discrepancy between theoretical and experimental result is attributable to the fact that in theoretical evaluation only the contribution of the LED, intended as a "stand-alone" object, is considered while in the experimental set-up is also considered the contribution of the receiver element since the experiment is based on the analysis of the sensor's voltage output. Therefore, to mathematically describe the effect of temperature variation on a single channel mid-IR sensor, both Emitter and Receiver spectral characteristics shall be considered simultaneously. Equation 3.4 describes the behaviour of a single channel InAsSb/InAs optopair [69], as the one used in the developed sensor.

$$A(\lambda, T) = P_{LED}(\lambda, T) \cdot R_{PD}(\lambda, T) \tag{3.4}$$

Equation 3.4 highlights that the sensor's output depends on how well the emission and detection spectra are spectrally matched. The More the two spectra overlap each other, higher the sensor's output is. If, due to temperature effect, one of the two spectra peak wavelength shifts, sensor's output would be affected. Solving Equation 3.4 for the Emitter temperature range 42 to 43 °C and considering the PD temperature at 27 °C, allows simulating the experimental set-up used for the analysis of temperature effect on emitter element (Figure 3.14). The result reported in Figure 3.15 shows that an increase of 1 °C reduces the output of 1.5%, while experimentally the increase of 1 °C reduces the output of 2%. Considering the approximation made by the mathematical model, this result confirms that the theoretical formulation correctly describes the behaviour observed experimentally.

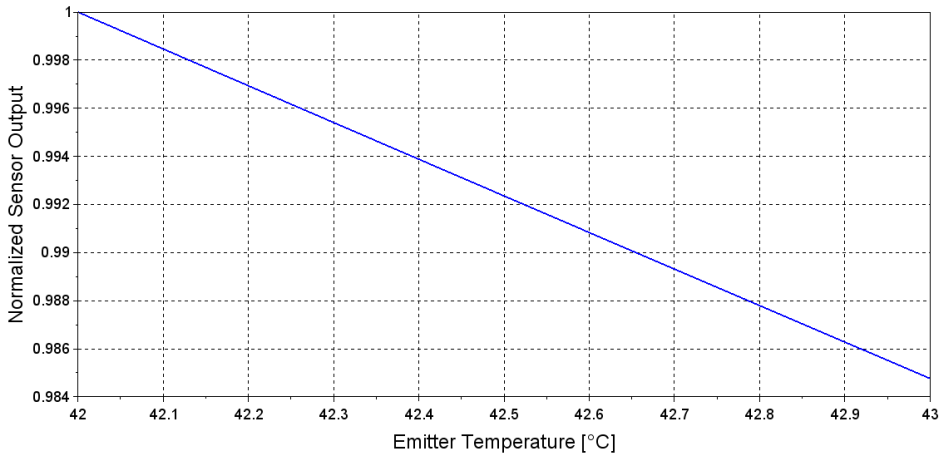

Figure 3.15: Theoretical evaluation of correlation between sensor's output and emitter element temperature, using sensor optopair formulation.

From the experiment has been estimated that the sensor output signal decreases of approximately 70 mV/°C. Considering that in our sensor, the output signal is reduced by approximately 700 mV at the maximum measurable value of CO_2 concentration, and considering the non-linearity of the sensor response described by 2.2, the above mentioned signal-temperature variability can not be tolerated. Further, a signal decrease due to LED temperature increase was noticed even if the heating system was turned off due to the LED's "self-heating" effect. The current circulating in the LED is sufficient to increase the optical element's temperature, thus

affecting its emitted power as discussed before. Therefore, a strategy to avoid the sensor signal variation due to the emitter stage's temperature variation is necessary.

3.3.4 Temperature Compensation

The results of the theoretical and experimental analysis suggest that temperature variations on the emitter stage represent the major contributor to output sensor signal variation, whereas the temperature effect on the sensitivity of the receiver can be considered negligible. Therefore, methods to compensate for the temperature variations on the emitter stage ware studied, in order to improve the output signal stability. At first, based on the linear regression obtained experimentally and reported in Figure 3.14, a compensation algorithm has been developed, as expressed in Equation 3.5:

$$Signal_{adjusted} = Signal_{filtered} + (T_{ref} - T_{filtered}) \cdot r \tag{3.5}$$

where $Signal_{adjusted}$ is the signal compensated for the temperature effect, $Signal_{filtered}$ is the output of the moving average filter applied to the acquired signal, T_{ref} is a reference temperature (mean value of the emitter stage temperature at steady state), $T_{filtered}$ is the output of the moving average filter applied to the temperature data. Since the temperature sensor is not placed next to the optical element but is in contact with the aluminium ring of the heating system, the temperature sensor's does not correctly describe the temperature dynamics of the optical elements. The reason is the thermal inertia introduced by the aluminium element that brings a delay in heat diffusion. Therefore, to correct the error in the acquisition of temperature data due to the temperature sensor's position, digital filtering has been implemented on optical and temperature signal. Two moving average filters with different windows width have been used to filter the acquired signal and the temperature. Using the above-mentioned filters allows compensation for the delay of the heat diffusion, and obtain temperature data that better describe the optical element temperature changes. The compensation algorithm's output has been further filtered through a moving average filter to improve signal stability. The proposed compensation algorithm allows the real-time correction of the signal acquired by the

sensor. In order to check efficiency of the proposed solution, compensation algorithm output has been compared to the optical signal filtered with a moving average filter, with filtering width of 90 samples (to compensate the temperature variation period of the sensor). The new solution based on the proposed compensation algorithm gives a result similar to the one obtained with the moving average in terms of signal stability (SD= + 6.29 mV vs SD= + 7.38 mV). Further, the compensation algorithm allows a shorter response time, as reported in Figure 3.16 in which a signal variation has been introduced applying a gas flow with CO_2 concentration of 2,5%. The increment of CO_2 causes the signal to decrease from approx. 3650 mV (signal value with environmental CO_2 concentration) to approx. 3200 mV. Further, as shown by Figure 3.16, without any compensation, due to thermal effect, the optical signal is characterized by high instability that reduces the accuracy of the sensor. Without any compensation, when a gas with CO_2 concentration of 2,5 % is applied at the sensor inlet, sensor's output is 2,5 % ± 1 %. With the proposed compensation method when a gas with CO_2 concentration of 2,5 % is applied at the sensor inlet, the concentration measured by the sensor is 2,5 % ± 0,1 %.

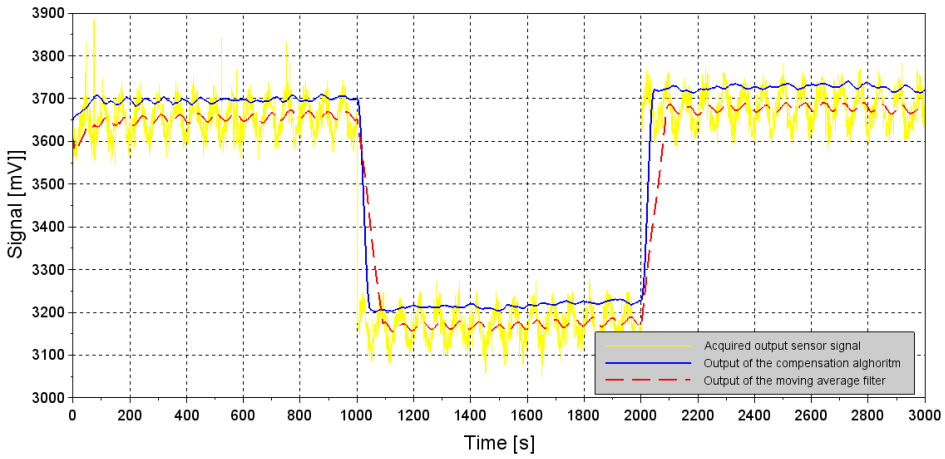

Figure 3.16: Comparison between the output of the compensation algorithm (blue) and the output of a moving average filter (dashed red). In yellow, the originally acquired output signal.

However, even though the proposed compensation algorithm allows to obtain a much stable output signal, the results in terms of sensor accuracy were not suffi-

ciently good. In particular, repeatability of the measurements with the same sensor was low, and the behaviour of different sensor was not the same. Reasons for that has been attributed to a different temperature-emitted optical power dependency for each InAsSb/InAs LED, and therefore a different r coefficient. Another reason for poor measurements repeatability can be found in different thermal conditions between the calibration and use phases. This means that the temperature acquired by the temperature sensor is not able to describe the optical element temperature effectively, probably due to its positioning and the thermal inertia introduced by the heating element. For these reasons, we decided to develop another method to obtain a stable and repeatable optical signal.

3.3.5 Temperature Control Algorithm

The previous results have highlighted that in order to have a stable optical signal, stable thermal conditions are necessary. Therefore, we developed a method that consists of an algorithm for generating periodical and controlled temperature variations on the emitter stage and synchronising the optical signal acquisition at known temperature conditions. In this way, the optical signal is always sampled at the same thermal conditions, and the signal variations due to heating–cooling dynamics are not taken into account. The developed algorithm is made of two phases:

- an initial phase performed at start-up, necessary to allow the sensor to reach the steady-state temperature, and
- a phase in which the heating module is alternatively turned on and off by the CPU.

The initial phase (`FIND_T_REG` state) is necessary to tune the control algorithm on the room temperature and to assure repeatability of the generated temperature oscillations used in the second phase. During the second phase, the CPU generates controlled temperature oscillations switching alternatively on and off the heating system. The heating system is switched off when the emitter stage temperature reaches a threshold value (HeaterRefT) based on the steady-state temperature. While the heating system is turned off (`ACQ_NO_HEATING` state) the output signal is acquired

and processed by the CPU through a moving average filter. This condition is maintained for a fixed duration of 45 s. Once the 45 s elapse the algorithm moves to the `WAIT_COOLING` state in which the signal acquisition is stopped, and the sensor output signal is no more updated. The heating system is maintained off during this state until a threshold value is reached (HeaterRefT - `HYST_TEMP_HEATER_OFF`). Further, in this state, the emitter LED is turned off to remove the LED self-heating due to the electrical current circulating. Once reached the threshold value, the algorithm moves to the `HEATING_NO_ACQ` state in which both the LED and heating system are turned on again. The algorithm then continues cyclically. A schematic representation of the algorithm is reported in Figure 3.17.

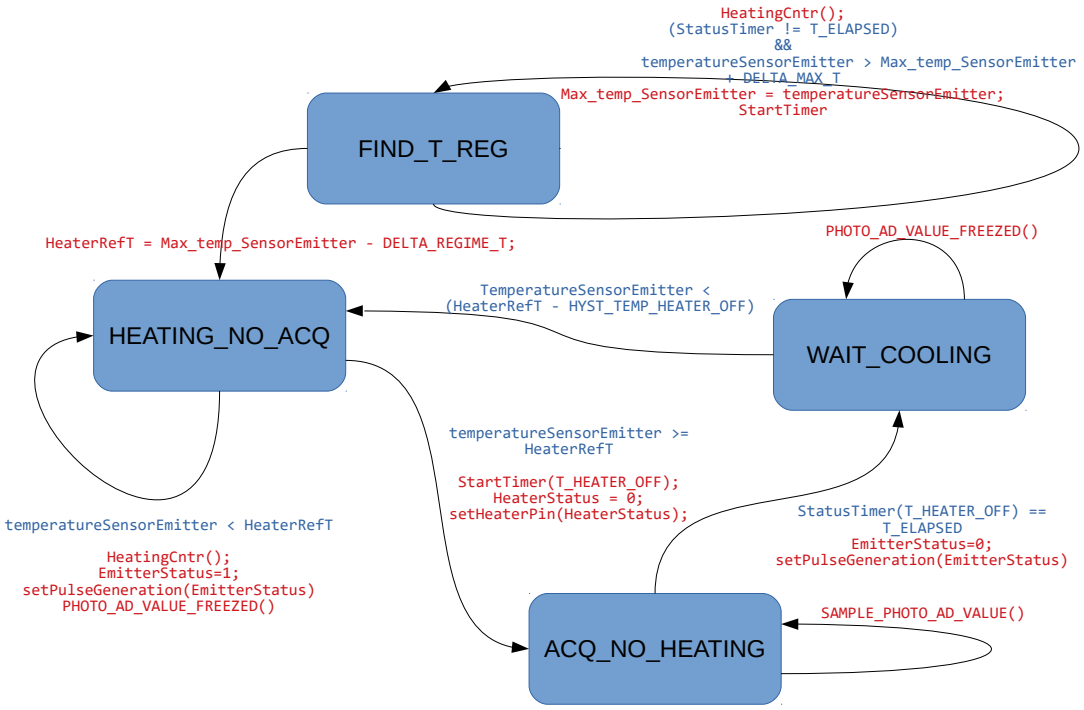

Figure 3.17: State diagram of Temperature Control Algorithm.

Through the proposed algorithm, the sensor output signal is updated only at the same thermal conditions; therefore, the output changes due to temperature variation are avoided. Outputs of the implemented algorithm are reported in Figures 3.18 and 3.19, in which the emitter stage temperature trend over time and the sensor output signal are shown respectively.

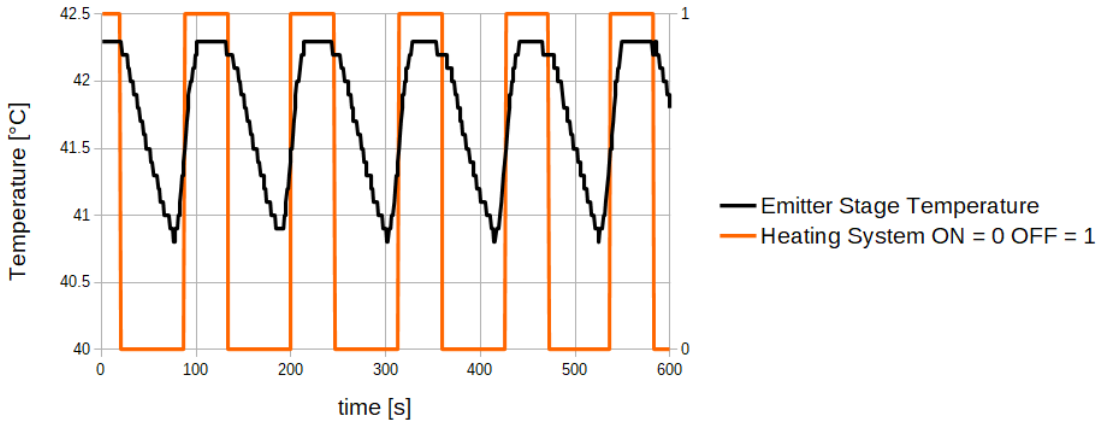

Figure 3.18: Emitter Stage Temperature trend obtained through the temperature control algorithm.

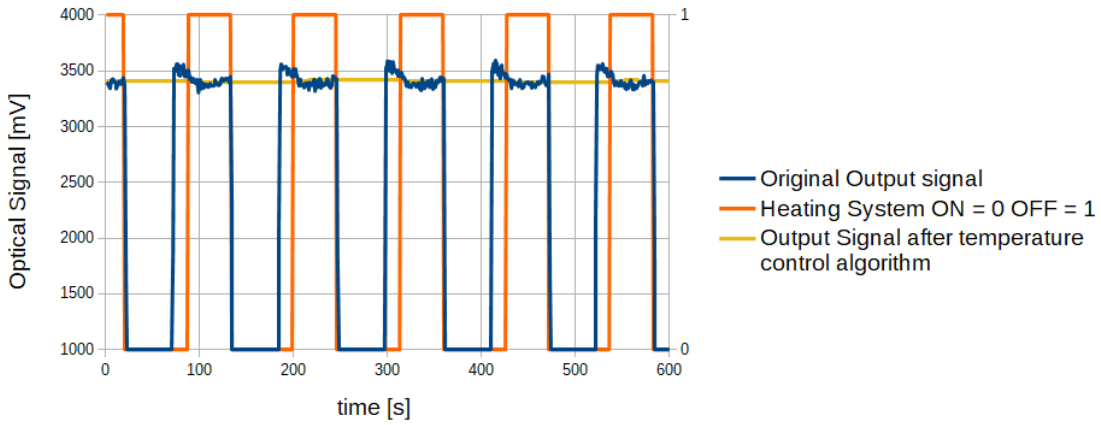

Figure 3.19: Original output signal (blue) and output signal (yellow) obtained through the temperature control algorithm.

As shown in Figure 3.18, the emitter stage temperature reaches the same values at each acquisition cycle (`HEATING_NO_ACQ` state). Therefore, as reported in 3.19, the output signal obtained through averaging operation of the signal acquired during the `HEATING_NO_ACQ` state is much more stable than the original signal. Without the implementation of the proposed algorithm, temperature dynamic on the emitter stage is characterized by oscillations without a defined period. Therefore, simple filtering methods such as a moving average on the acquired signal result poorly effective as the temperature–signal dependency remains.

Chapter 4

Sensor Validation

The developed sensor and the algorithm described in section 3.3.5 have been validated both in-vitro and in-vivo. In this chapter, the results of the tests performed on the developed CO_2 sensor are reported.

4.1 Sensor Validation in Experimental Laboratory Setting

At first, the developed sensor has been tested in an experimental laboratory setting. Before testing, the sensor was calibrated by using gas tanks containing gas mixtures of air and CO_2 with known concentrations. The measurement range for CO_2 concentration was 0–9%, as the developed sensor is intended to be used for treating patients in hypercapnic conditions (i.e. P_aCO_2 higher than 50 mmHg [86], corresponding to a CO_2 concentration of approximately 6.5%). The gas was let flow through the sensor, and the output signal was recorded through a PC connected to the sensor via RS-485 communication line. The following CO_2 concentrations were used for the calibration procedure; 0%, 2.5%, 5%, 7.5%, and 9%. The collected data were used to obtain a calibration curve through polynomial interpolation. Example of a calibration curve is reported in Figure 4.1.

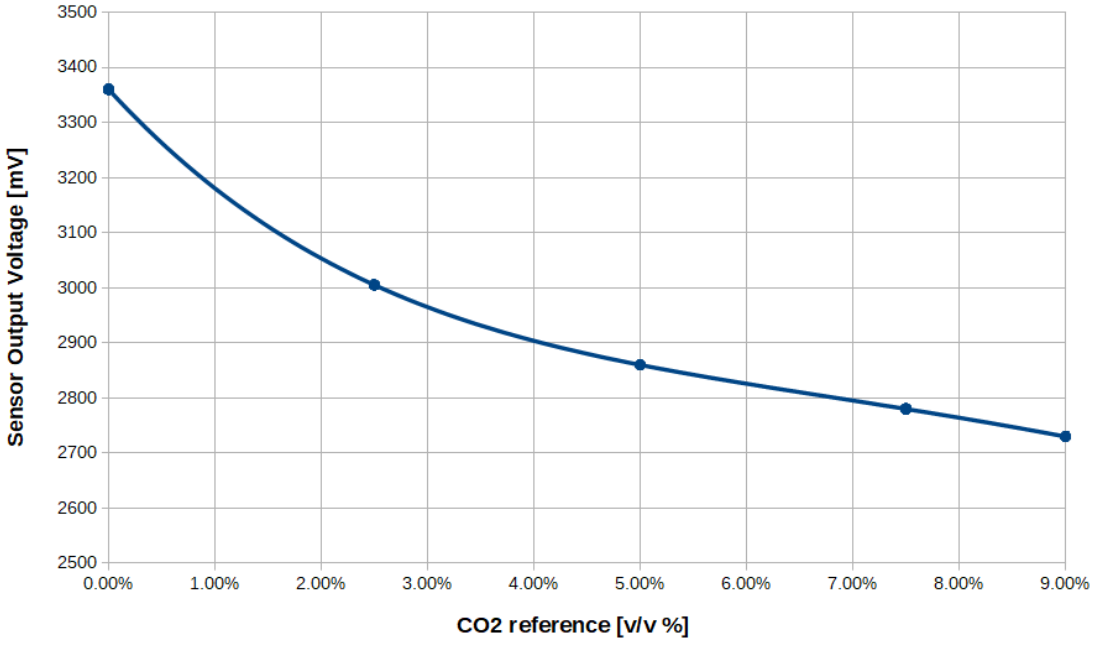

Figure 4.1: Example of calibration curve. Dots represent the values used for polynomial interpolation.

Values of the interpolation curve relevant to the measurement range with resolution step of 0.1%, have been then stored in the sensor's flash memory. Through the calibration table stored in its flash memory, the sensor is then able to convert the output signal in CO_2 concentration value, as a percentage value. Calibration process is intended as a "one-time" operation, considering also that at each use of the sensor, a "Zero" value is acquired in absence of CO_2, and used for offset correction. At this time no evidence that the sensor will need a periodic calibration have been gathered. If periodic calibration will be necessary, this operation can be easily carried out, since the calibration data can be loaded on sensor's flash memeory through serial communication port, without invasive operations on sensor's electronic or optical parts. The developed sensor's accuracy was verified by comparing its measurement with the ones obtained by a "gold standard" device (Medtronic Microcap Plus Capnograph). The two sensors' accuracy was compared using a mixture of air and CO_2 at several concentrations. In order to control the CO_2 concentration of the gas mixture used for the test, it was analysed through a bench gas analyser (Servomex MiniMP 5200). In Table 4.1 are reported the data gathered during the

test execution.

Table 4.1: Comparison between measurements got by the developed sensor and a "gold standard" device for several CO_2 concentration values. Error is expressed as average value and standard deviation (SD).

CO_2 set-point [v/v %]	Developed CO_2 Sensor	"Gold Standard" Sensor
1.60 %	1.60 %	1.40 %
2.20 %	2.00 %	1.90 %
3.60 %	3.50 %	3.40 %
3.90 %	4.00 %	4.00 %
5.40 %	5.50 %	5.30 %
6.10 %	5.80 %	6.20 %
6.60 %	6.50 %	6.70 %
7.40 %	7.50 %	7.50 %
Average Error ± SD [v/v %]	0.13 ± 0.09%	0.15 ± 0.07 %

From data reported in the table, the average absolute error obtained for the newly developed sensor (0.13%) is similar to the one obtained by the reference device (0.15%), that is already validated for clinical practice. Further, the developed sensor's accuracy level complies with requirements prescribed by ISO 80601-2-55 as reported in Figure 4.2. These results demonstrate the efficiency of the temperature control algorithm in terms of output signal stability, therefore the developed sensor's reliability.

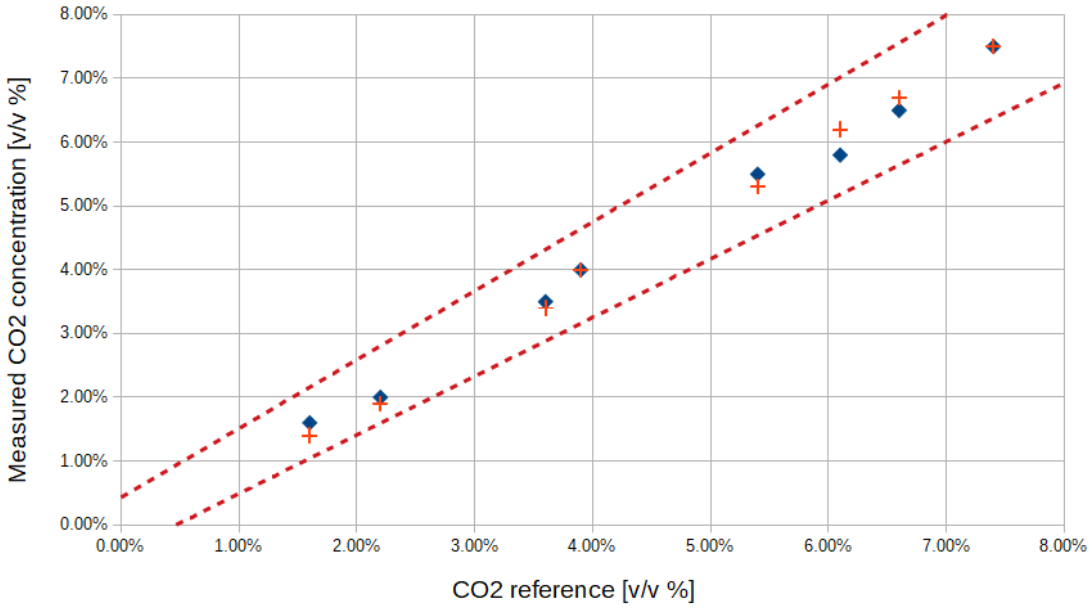

Figure 4.2: CO_2 concentration measurement provided by the newly developed sensor (blue diamonds) and by the "gold standard" device (orange crosses). Dashed lines represent the ISO 80601-2-55 error limits.

Sensor accuracy has also been evaluated comparing the measurement of twelve sensors at several CO_2 concentration level. The acquired values are reported in the following table.

Table 4.2: Evaluation of developed sensor accuracy, comparing the output of twelve sensors.

Sensor ID	CO_2=0%	CO_2=2,5%	CO_2=5%	CO_2=7,5%	CO_2=9%
1	0,0%	2,2%	4,6%	7,1%	8,3%
2	0,0%	2,3%	4,7%	6,7%	8,4%
3	0,0%	2,4%	5,0%	7,7%	8,8%
4	0,0%	2,4%	5,1%	7,5%	8,9%
5	0,0%	2,7%	5,2%	7,6%	9,0%
6	0,0%	2,4%	5,0%	7,7%	8,8%
7	0,0%	2,7%	4,9%	7,6%	8,8%
8	0,2%	2,6%	5,1%	7,9%	9,0%
9	0,0%	2,5%	5,0%	7,6%	9,0%
10	0,0%	2,4%	5,2%	7,5%	9,0%
11	0,0%	2,5%	5,5%	7,5%	9,0%
12	0,1%	2,7%	5,1%	7,3%	9,0%
Average ± SD [v/v %]	0,0 ± 0,0%	2,5 ± 0,2%	5 ± 0,2%	7,5 ± 0,3%	8,8 ± 0,2%

Converting the results reported in Table 4.2 in mmHg, the sensor accuracy is: ± 1,5mmHg in the range 0-38 mmhHg, ± 2,3 mmHg in the range 39-57 mmHg, and ± 3 mmHg in the range 58-68 mmHg. Therefore, the developed CO_2sensor's performance can be considered similar to the performance of the capnometers for respiratory monitoring reported in section 2.3.

4.2 In-Vivo Sensor Validation

Since the project's goal was to develop a CO_2 sensor for ECLS applications with TRL of 9, validation of the product in its intended operational environment was necessary. For this reason, we tested the developed CO_2 sensor through in-vivo experiment. The developed CO_2 sensor has been tested in an animal model and the acquired data compared with the ones taken with Medtronic Microcap Plus Capnograph. Data were collected during the execution of experiments described in [58], in which

five pigs with induced cardiogenic shock were undergoing ECMO procedure. This experiment was conducted as part of a major study aimed at comparing the effects of treatments alone with VA ECMO in addition to intra-aortic balloon pump (IABP) in pigs in cardiogenic shock. Data were obtained on the five pigs, at five different levels of blood flow/gas flow ratio (between 0.5-1.5). Three data acquisition were made for each level of blood flow/gas flow ratio. Acquired data are reported in Table 4.3 (only one data set for each level of blood flow/gas flow ratio is reported). Measurements from the newly developed capnometer and the reference device were taken at the MO exhaust port. Further, the GF measurement taken at the inlet port of the MO through our flow sensor and the one provided by a reference device were compared. Finally, VCO_2 data obtained by CO_2 measurement from our system were evaluated against VCO_2 calculated through data gathered by the reference device. VCO_2 values have been calculated using Equation 1.2. As during in-vivo tests the CO_2 concentration cannot be set arbitrarily, but instead depends on the effectiveness of the ECMO procedures and on parameters such as sweep gas flow and blood flow, to validate our sensor we focused on the error obtained comparing the measurements from our sensor with the ones taken with the reference device, that is routinely used in clinical practice. The reference device considered is a CO_2 sensor intended for respiratory monitoring, and it can perform the measurements only in "intermittent" gas flow conditions like breathing. Therefore, during our experiments, the reference device was manually connected/disconnected from the MO exhaust port.

Results are reported in Table 4.3.

Table 4.3: Error between measurement taken with the newly developed system and the "gold standard" devices for CO_2 concentration, Gas Flow, and VCO_2. Error is expressed as average value and standard deviation (SD).

Animal ID	Blood Flow / Gas Flow ratio	Gas Flow Developed Sensor {[}l/min]	Gas Flow "Gold Standard" {Sensor []l/min]	CO\textsubscript{2} Concentration Developed Sensor {[}v/v %]	CO\textsubscript{2} Concentration "Gold Standard" {Sensor []v/v %]	VCO\textsubscript{2} Developed Sensor {[}ml/min]	VCO\textsubscript{2} "Gold Standard" {Sensor []ml/min]
	1/0,5	1,60	1,50	3,80	3,80	60,8	57,0
	1/0,7	1,80	1,75	3,80	3,80	68,4	66,5
#1	1/1	3,10	3,00	2,80	3,00	86,8	90,0
	1/1,2	2,40	2,40	3,40	3,30	81,6	79,2
	1/1,5	3,10	3,00	3,00	3,00	93,0	90,0
	1/0,5	1,00	1,00	7,00	6,90	70,0	69,0
	1/0,7	1,40	1,40	6,00	5,90	84,0	82,6
#2	1/1	2,10	2,00	5,00	4,90	105,0	98,0
	1/1,2	3,80	3,60	3,60	3,60	136,8	129,6
	1/1,5	3,10	3,00	4,20	4,20	130,2	126,0
	1/0,5	1,00	1,00	6,80	6,80	68,0	68,0
	1/0,7	1,40	1,40	6,20	6,30	86,8	88,2
#3	1/1	2,00	2,00	5,40	5,20	108,0	104,0
	1/1,2	2,40	2,40	4,40	4,50	105,6	108,0
	1/1,5	3,10	3,00	3,80	3,90	117,8	117,0
	1/0,5	1,10	1,00	8,20	8,30	90,2	83,0
	1/0,7	1,50	1,40	7,60	7,60	114,0	106,4
#4	1/1	2,00	2,00	7,00	7,00	140,0	140,0
	1/1,2	2,40	2,40	5,80	5,70	139,2	136,8
	1/1,5	3,10	3,00	5,20	5,10	161,2	153,0
	1/0,5	1,60	1,50	5,00	4,90	80,0	73,5
	1/0,7	2,20	2,10	4,60	4,60	101,2	96,6
#5	1/1	3,10	30	3,80	3,70	117,8	111,0
	1/1,2	3,60	3,60	3,40	3,40	122,4	122,4
	1/1,5	4,50	4,50	3,30	3,40	148,5	153,0
		Gas Flow Average Error ± SD [l/min]		CO2 Concentration Average Error ± SD [v/v %]		VCO2 Average Error ± SD [ml/min]	
		0.06 ± 0.05		0.07 ± 0.06		3,66 ± 2,6	

As reported in Table 4.3, the difference for GF, CO_2 and VCO_2 between the developed sensor and the reference instrument is minimal. Therefore, these results show that the developed CO_2 sensor represents a reliable solution in the clinical environment. Further, a similar error has been obtained both in in-vitro and in-vivo tests for CO_2 concentration. This result is significant since the main difference between the two set-ups consists of the presence of water vapour in the oxygenator exhaust. Therefore, the heating system implemented in the CO_2 sensor to avoid water vapour condensation, and relevant algorithm for temperature control, are valid solutions. This is true even in long-term measurements since, during the in-vivo test, the sensor has been able to work for several days without showing any form of signal degradation. The results obtained through the in-vivo test demonstrated that the developed sensor is functional in its intended environment of use, therefore reaching the TRL 9, achieving the project goal. Based on the results obtained both laboratory and clinical environment, the developed sensor has obtained the CE mark. To date, approximately 150 sensors have been produced and distributed and are currently used in intensive care units connected to multi-parametric monitoring systems for ECMO procedures and to ECCO2R devices.

Chapter 5

Conclusion

ECLS procedures have become more and more important over the years, and their use has increased in the recent period due to the Covid-19 pandemic. Therefore methods to enhance both safety and effectiveness of the extra corporeal procedure are needed. All ECLS procedures involve a membrane oxygenator that totally or partially substitutes the patient's lung functionality, allowing both blood oxygenation and carbon dioxide removal. Measurement of CO_2 concentration in the exhaust gas of a membrane oxygenator allows monitoring both patient's status during the ECLS procedure and the state of the membrane oxygenator and its performance. Therefore, oxygenator exhaust capnometry represents a useful tool that allows correct management of the ECLS procedure and improves its safety, assuring a better patient outcome. In this thesis, the development of a sensor specifically designed to measure carbon dioxide concentration in the exhaust gas of a membrane oxygenator during extra corporeal procedures is presented. The PhD project's goal is not only the development of a sensor prototype but also the development of a sensor with Technology Readiness Level of 9, meaning that the developed sensor shall also be proven and validated in the operational environment. The developed sensor is made up by two sections: one for measurement of the gas flow applied to a membrane oxygenator, and the other for the measurement of carbon dioxide concentration in the exhaust gas, which represents the CO_2 removed from the patient's blood. The proposed CO_2 sensor is designed as a Main Stream sensor with a single channel optical architecture, avoiding the use of optical filters and therefore obtaining a sim-

ple, cheap and easy to assemble the system. As a high amount of water vapour characterizes the oxygenator exhaust gas, condensation at the exhaust connector is easy to occur. Therefore, in order to avoid water vapour condensation within the optical sensor, with consequent degradation of the optical signal, a heating module is implemented in the CO_2 measurement section. Even though the implemented heating system prevents water vapour condensation, temperature variations affect the optical elements' performance. Temperature effect on the optical elements used in the CO_2 sensor was analyzed both theoretically and experimentally, highlighting the strong correlation between emitter LED temperature and acquired optical signal. Even though both theoretical and experimental results highlight a negative correlation between emitted optical power and emitter stage temperature, the two relationships are characterized by different slopes. This result can be explained, considering that, in the experimental setup, the sensor photodiode contributes to the variation of the sensor's output. In contrast, this contribution is not taken into account in the theoretical formulation, as the emitter element is considered a "stand-alone" component. To correctly describe the experimental setup, the formulation reported in Equation 3.4 has been used. This formulation considers both the emitter and receiver contribute to the sensor output, thus describing the sensor optopair. Using it to simulate the experimental setup, the obtained relationship between sensor output and emitter temperature is close to the one obtained experimentally. The mathematical model used was confirmed valid and useful to evaluate the effect of temperature changes introduced by the implemented heating system on the optical elements. Further, as reported in [85], the mathematical model can also be used to evaluate sensor sensitivity. Therefore, the adopted mathematical model represents the basis for further improvement of the developed device since it allows the exploration of our sensor's behaviour for different conditions of use, e.g., higher temperatures, different optical path length, and higher CO_2 concentration. In order to remove the signal–temperature dependency and therefore improve sensor sensitivity, an algorithm for heating system control was implemented. The proposed solution consists in the generation of controlled and repeatable temperature oscillations and acquisition of the sensor's output signal always at the same thermal

conditions. Use of the proposed temperature control algorithm results in a stable output signal since only samples acquired at the same thermal conditions are considered. The main drawback of the implemented solution is the low time resolution of the measurement. Considering the duration of a thermal cycle, there is a 90 seconds delay in the detection of a CO_2 concentration variation. However, this delay does not represent a major problem considering that the sensor is intended for long term therapy that lasts for days or weeks, meaning that the data gathered through the sensors are used to get long-term information about therapy progress and trends. The developed sensor's accuracy has been compared against a CO_2 sensor used in clinical practice both through laboratory test and in-vivo test. The results show that the developed system allows reliable measurement of gas flow and carbon dioxide concentration, and therefore of carbon dioxide removal rate VCO_2. Therefore, the developed sensor has been validated in in its intended operational environment, achieving a technology readiness level equal to 9. As far as the author knows, only other two devices for measuring of CO_2 concentration specifically designed for ECLS application are available at the moment, the CO_2 sensor of Spectrum M4 system (Spectrum Medical Ltd.) and the Hemolung RAS ECCO2R device (A-Lung Technologies, Inc.). Unfortunately, from the available documentation no information about their performances in terms of CO_2 concentration accuracy was found, nor was it possible to compare them with the developed sensor experimentally. Spectrum M4 system CO_2 sensor is based on the same optical principle exploited by the developed sensor, and it seems designed as a "Main Stream" sensors, suitable for connection to the exhaust port of the membrane oxygenator. Anyway, in the available documentation, the adopted solution to address the water vapor condensation problem is not described. Further, similar to the developed sensor also the Spectrum M4 system is designed as a double section architecture, with a gas flow measurement section intended to be placed upstream of the membrane oxygenator, and the CO_2 sensor connected to the exhaust port. Finally, the Spectrum M4 system calculates the PCO_2 value of the blood leaving the oxygenator. This value is obtained through a proprietary algorithm based on the value measured by the CO_2 sensor and to the measurement of the atmospheric pressure. Future improvement of the developed

sensor should involve the development of an algorithm for estimation of the PCO_2 value from the CO_2 concentration measured in the exhaust gas. The developed sensor fulfils the requirements prescribed by ISO 80601-2-55 standard relevant to the accuracy of carbon dioxide concentration measurements and has obtained the CE mark. Approximately 150 sensors have been produced and distributed, and they are currently used in intensive care units connected to multi-parametric monitoring systems for ECMO procedures and to $ECCO_2R$ devices.

Bibliography

[1] Daniel P Davis. Quantitative capnometry as a critical resuscitation tool. *Journal of Trauma Nursing*, 12(2):40, 2005.

[2] Francisco José Cereceda-Sánchez and Jesús Molina-Mula. Systematic review of capnography with mask ventilation during cardiopulmonary resuscitation maneuvers. *Journal of clinical medicine*, 8(3):358, 2019.

[3] Naveen Eipe and Dermot R Doherty. A review of pediatric capnography. *Journal of clinical monitoring and computing*, 24(4):261–268, 2010.

[4] Štefek Grmec. Comparison of three different methods to confirm tracheal tube placement in emergency intubation. *Intensive care medicine*, 28(6):701–704, 2002.

[5] Dejan Kupnik and Pavel Skok. Capnometry in the prehospital setting: are we using its potential? *Emergency Medicine Journal*, 24(9):614–617, 2007.

[6] Steven A Conrad, L Mikael Broman, Fabio S Taccone, Roberto Lorusso, Maximilian V Malfertheiner, Federico Pappalardo, Matteo Di Nardo, Mirko Belliato, Lorenzo Grazioli, Ryan P Barbaro, et al. The extracorporeal life support organization maastricht treaty for nomenclature in extracorporeal life support. a position paper of the extracorporeal life support organization. *American journal of respiratory and critical care medicine*, 198(4):447–451, 2018.

[7] RH Bartlett, L Gattinoni, et al. Current status of extracorporeal life support (ecmo) for cardiopulmonary failure. *Minerva Anestesiol*, 76(7):534–540, 2010.

[8] Extracorporeal Life Support Organization (ELSO). Ecls registry report, international summary, July, 2020.

[9] Mihály Héder. From nasa to eu: the evolution of the trl scale in public sector innovation. *The Innovation Journal*, 22(2):1–23, 2017.

[10] David Machin and Chris Allsager. Principles of cardiopulmonary bypass. *Continuing Education in Anaesthesia, Critical Care & Pain*, 6(5):176–181, 2006.

[11] Robert C Groom, David Fitzgerald, Jacob T Gutsche, and Harish Ramakrishna. Extracorporeal devices including extracorporeal membrane oxygenation. In *Kaplan's Essentials of Cardiac Anesthesia for Cardiac Surgery*, pages 664–684. Elsevier Inc., 2017.

[12] Ali Ostadfar. *Biofluid mechanics: Principles and applications*. Academic Press, 2016.

[13] John M Toomasian and Robert H Bartlett. Hemolysis and ecmo pumps in the 21st century. *Perfusion*, 26(1):5, 2011.

[14] Gerhard Ziemer and Axel Haverich. *Cardiac Surgery: Operations on the Heart and Great Vessels in Adults and Children*. Springer, 2017.

[15] Glenn P Gravlee. *Cardiopulmonary bypass: principles and practice*. Lippincott Williams & Wilkins, 2008.

[16] RS Kramer, JR Morton, RC Groom, and DL Robaczewski. Coronary artery bypass grafting. 2018.

[17] Kenneth M TAYLOR. Cardiopulmonary bypass principles and management. *15 Blood cell trauma*, pages 249–276, 1986.

[18] K Mottaghy, B Oedekoven, H Starmans, B Müller, A Kashefi, B Hoffmann, and S Böhm. Technical aspects of plasma leakage prevention in microporous capillary membrane oxygenators. *ASAIO Journal*, 35(3):640–643, 1989.

[19] J Patrick Montoya, Charles J Shanley, Scott I Merz, and Robert H Bartlett. Plasma leakage through microporous membranes. role of phospholipids. *Asaio Journal (American Society for Artificial Internal Organs: 1992)*, 38(3):M399–405, 1992.

[20] Marcelo Cypel and Shaf Keshavjee. Artificial lung support. In *Regenerative Medicine Applications in Organ Transplantation*, pages 683–689. Elsevier, 2014.

[21] Heidi J Dalton and Warwick W Butt. Extracorporeal life support: an update of rogers' textbook of pediatric intensive care. *Pediatric Critical Care Medicine*, 13(4):461–471, 2012.

[22] Manjula Sarkar and Vishal Prabhu. Basics of cardiopulmonary bypass. *Indian journal of anaesthesia*, 61(9):760, 2017.

[23] Frederick A Hensley, Donald Eugene Martin, and Glenn P Gravlee. *A practical approach to cardiac anesthesia*. Lippincott Williams & Wilkins, 2012.

[24] Brian Freeman and Jeffrey Berger. *Anesthesiology Core Review*. McGraw-Hill Education, 2014.

[25] Jan W de Jong. Cardioplegia and calcium antagonists: a review. *The Annals of thoracic surgery*, 42(5):593–598, 1986.

[26] Vladimir Svitek, Vladimir Lonsky, and Faraz Anjum. Pathophysiological aspects of cardiotomy suction usage. *Perfusion*, 25(3):147–152, 2010.

[27] Silvana F Marasco, George Lukas, Michael McDonald, James McMillan, and Benno Ihle. Review of ecmo (extra corporeal membrane oxygenation) support in critically ill adult patients. *Heart, Lung and Circulation*, 17:S41–S47, 2008.

[28] John J Squiers, Brian Lima, and J Michael DiMaio. Contemporary extracorporeal membrane oxygenation therapy in adults: fundamental principles and systematic review of the evidence. *The Journal of thoracic and cardiovascular surgery*, 152(1):20–32, 2016.

[29] Steve Allen, Daniel Holena, Maureen McCunn, Benjamin Kohl, and Babak Sarani. A review of the fundamental principles and evidence base in the use of extracorporeal membrane oxygenation (ecmo) in critically ill adult patients. *Journal of intensive care medicine*, 26(1):13–26, 2011.

[30] Preston B Rich, Samir S Awad, Stefania Crotti, Ronald B Hirschl, Robert H Bartlett, and Robert J Schreiner. A prospective comparison of atrio-femoral and femoro-atrial flow in adult venovenous extracorporeal life support. *The Journal of thoracic and cardiovascular surgery*, 116(4):628–632, 1998.

[31] Christian A Bermudez, Rodolfo V Rocha, Penny L Sappington, Yoshiya Toyoda, Holt N Murray, and Arthur J Boujoukos. Initial experience with single cannulation for venovenous extracorporeal oxygenation in adults. *The Annals of thoracic surgery*, 90(3):991–995, 2010.

[32] Available at:. `https://www.euroelso.net/covid-19/covid-19-survey/`. Accessed: 2020-12-12.

[33] Kiran Shekar, Jenelle Badulak, Giles Peek, Udo Boeken, Heidi J Dalton, Lovkesh Arora, Bishoy Zakhary, Kollengode Ramanathan, Joanne Starr, Bindu Akkanti, et al. Extracorporeal life support organization coronavirus disease 2019 interim guidelines: A consensus document from an international group of interdisciplinary extracorporeal membrane oxygenation providers. *Asaio Journal*, 2020.

[34] Xiaoyang Hong, Jing Xiong, Zhichun Feng, and Yuan Shi. Extracorporeal membrane oxygenation (ecmo): does it have a role in the treatment of severe covid-19? *International Journal of Infectious Diseases*, 2020.

[35] Available at:. `https://www.elso.org/Registry/FullCOVID19RegistryDashboard.aspx`. Accessed: 2020-12-12.

[36] L Gattinoni, T Kolobow, G Damia, A Agostoni, and A Pesenti. Extracorporeal carbon dioxide removal (ecco 2r): a new form of respiratory assistance. *International Journal of Artificial Organs*, 2(4):183–185, 1979.

[37] Lorenzo Del Sorbo, Marcelo Cypel, and Eddy Fan. Extracorporeal life support for adults with severe acute respiratory failure. *The Lancet Respiratory Medicine*, 2(2):154–164, 2014.

[38] Philippe Morimont, Andriy Batchinsky, and Bernard Lambermont. Update on the role of extracorporeal co 2 removal as an adjunct to mechanical ventilation in ards. *Critical Care*, 19(1):1–7, 2015.

[39] Luigi Camporota and Nicholas Barrett. Current applications for the use of extracorporeal carbon dioxide removal in critically ill patients. *BioMed Research International*, 2016, 2016.

[40] Christian Karagiannidis, Kristin Aufm Kampe, Fernando Suarez Sipmann, Anders Larsson, Goran Hedenstierna, Wolfram Windisch, and Thomas Mueller. Veno-venous extracorporeal co 2 removal for the treatment of severe respiratory acidosis: pathophysiological and technical considerations. *Critical care*, 18(3):1–10, 2014.

[41] Hadrien Winiszewski, François Aptel, François Belon, Nicolas Belin, Claire Chaignat, Cyrille Patry, Cecilia Clermont, Elise David, Jean-Christophe Navellou, Guylaine Labro, et al. Daily use of extracorporeal co 2 removal in a critical care unit: indications and results. *Journal of intensive care*, 6(1):36, 2018.

[42] Andrea Morelli, Lorenzo Del Sorbo, Antonio Pesenti, V Marco Ranieri, and Eddy Fan. Extracorporeal carbon dioxide removal (ecco 2 r) in patients with acute respiratory failure. *Intensive care medicine*, 43(4):519–530, 2017.

[43] RC Tasker and MJ Peters. Combined lung injury, meningitis and cerebral edema: how permissive can hypercapnia be? *Intensive care medicine*, 24(6):616, 1998.

[44] Milan Stengl, Lenka Ledvinova, Jiri Chvojka, Jan Benes, Dagmar Jarkovska, Jaromir Holas, Patrik Soukup, Jitka Sviglerová, and Martin Matejovic. Effects of clinically relevant acute hypercapnic and metabolic acidosis on the cardio-

vascular system: an experimental porcine study. *Critical Care*, 17(6):R303, 2013.

[45] Robert A Baker, Shahna L Bronson, Timothy A Dickinson, David C Fitzgerald, Donald S Likosky, Nicholas B Mellas, Kenneth G Shann, et al. Report from amsect's international consortium for evidence-based perfusion: American society of extracorporeal technology standards and guidelines for perfusion practice: 2013. *The journal of extra-corporeal technology*, 45(3):156, 2013.

[46] Karlman Wasserman, Brian J Whipp, and Richard Casaburi. Respiratory control during exercise. *Comprehensive Physiology*, pages 595–619, 2011.

[47] Vito Fanelli, Andrea Costamagna, Pierpaolo P Terragni, and V Marco Ranieri. Low-flow ecmo and co 2 removal. In *ECMO-Extracorporeal Life Support in Adults*, pages 303–315. Springer, 2014.

[48] R Peter Alston, Neil J Glassford, and Amanda Torrie. Measurement of systemic carbon dioxide production during cardiopulmonary bypass: a comparison of fick's principle with oxygentor exhaust output. *Perfusion*, 18(6):339–344, 2003.

[49] Marco Ranucci, Giovanni Carboni, Mauro Cotza, and Filip De Somer. Carbon dioxide production during cardiopulmonary bypass: pathophysiology, measure and clinical relevance. *Perfusion*, 32(1):4–12, 2017.

[50] Anne Louise Bellaiche, Peter F Nielsen, Steven Brantlov, Marianne B Møller, and Michael Winterdahl. Clinical evaluation of the accuracy and precision of the cdi 500 in-line blood gas monitor with and without gas calibration. *The journal of extra-corporeal technology*, 43(2):53, 2011.

[51] Christian Brendle, K-F Hackmack, Jan Kühn, MN Wardeh, Thorsten Janisch, Rüdiger Kopp, Rolf Rossaint, André Stollenwerk, Stefan Kowalewski, B Misgeld, et al. Continuous gas transfer monitoring during extracorporeal membrane oxygenation. *Biomedical Signal Processing and Control*, 31:321–330, 2017.

[52] Kieron C Potger, Darryl McMillan, Joanne Southwell, Hayden Dando, and Killian O Shaughnessy. Membrane oxygenator exhaust capnography for con-

tinuously estimating arterial carbon dioxide tension during cardiopulmonary bypass. *Journal of ExtraCorporeal Technology*, 35(3):218–223, 2003.

[53] MJ O'Leary, SP MacDonnell, and CN Ferguson. Oxygenator exhaust capnography as an index of arterial carbon dioxide tension during cardiopulmonary bypass using a membrane oxygenator. *British journal of anaesthesia*, 82(6):843–846, 1999.

[54] RP Alston and J McNicol. Oxygenator exhaust capnography: An in vitro evaluation. *Journal of cardiothoracic anesthesia*, 2(6):798–802, 1988.

[55] Marco Ranucci, Giuseppe Isgrò, Federica Romitti, Sara Mele, Bonizella Biagioli, and Pierpaolo Giomarelli. Anaerobic metabolism during cardiopulmonary bypass: predictive value of carbon dioxide derived parameters. *The Annals of thoracic surgery*, 81(6):2189–2195, 2006.

[56] Filip De Somer, John W Mulholland, Megan R Bryan, Tommaso Aloisio, Guido J Van Nooten, and Marco Ranucci. O 2 delivery and co 2 production during cardiopulmonary bypass as determinants of acute kidney injury: time for a goal-directed perfusion management? *Critical care*, 15(4):R192, 2011.

[57] Ravi R Thiagarajan, Ryan P Barbaro, Peter T Rycus, D Michael Mcmullan, Steven A Conrad, James D Fortenberry, Matthew L Paden, et al. Extracorporeal life support organization registry international report 2016. *ASAIO journal*, 63(1):60–67, 2017.

[58] Alice Montalti, Mirko Belliato, Sandro Gelsomino, Sandro Nalon, Francesco Matteucci, Orlando Parise, Monique de Jong, Maged Makhoul, Daniel M Johnson, and Roberto Lorusso. Continuous monitoring of membrane lung carbon dioxide removal during ecmo: experimental testing of a new volumetric capnometer. *Perfusion*, page 538–543, 2019.

[59] Francesco Epis and Mirko Belliato. Oxygenator performance and artificial-native lung interaction. *Journal of thoracic disease*, 10(Suppl 5):S596, 2018.

[60] Jane Hodgkinson and Ralph P Tatam. Optical gas sensing: a review. *Measurement Science and Technology*, 24(1):012004, 2012.

[61] Barbara Stuart. Infrared spectroscopy. *Kirk-Othmer Encyclopedia of Chemical Technology*, pages 1–18, 2000.

[62] Trieu-Vuong Dinh, In-Young Choi, Youn-Suk Son, and Jo-Chun Kim. A review on non-dispersive infrared gas sensors: Improvement of sensor detection limit and interference correction. *Sensors and Actuators B: Chemical*, 231:529–538, 2016.

[63] TV Bezyazychnaya, MV Bogdanovich, VV Kabanov, DM Kabanau, YV Lebiadok, VV Parashchuk, AG Ryabtsev, GI Ryabtsev, PV Shpak, MA Shchemelev, et al. Light emitting diode–photodiode optoelectronic pairs based on the inas/inassb/inassbp heterostructure for the detection of carbon dioxide. *Semiconductors*, 49(7):980–983, 2015.

[64] Iouli E Gordon, Laurence S Rothman, Christian Hill, Roman V Kochanov, Y Tan, Peter F Bernath, Manfred Birk, V Boudon, Alain Campargue, KV Chance, et al. The hitran2016 molecular spectroscopic database. *Journal of Quantitative Spectroscopy and Radiative Transfer*, 203:3–69, 2017.

[65] Martin Degner, Henning Jürß, and Hartmut Ewald. Fast and low power optical co 2-sensors for medical application: New sensor designs for main-and side-stream co 2-sensors are presented in comparison with state of the art capnometers. In *2018 IEEE International Instrumentation and Measurement Technology Conference (I2MTC)*, pages 1–5. IEEE, 2018.

[66] Rodney J. Solomon. Ta reliable, accurate co2 analyzer for medical use. *Hewlett-Packard Journal*, 32:3–21, 1981.

[67] Horst-Dieter Hattendorff, Bernd Grabbet, Eberhart Liesching, and Regina Best. Sensor arrangement for optically measuring gas components, March 3 1992. US Patent 5,092,342.

[68] Roger Susi, Arthur R Weeks, David Hefele, and John Moore. Anesthetic gas detection apparatus, August 21 2001. US Patent 6,277,081.

[69] Galina Yu Sotnikova, Gennadyy A Gavrilov, Sergey E Aleksandrov, Alexander A Kapralov, Sergey A Karandashev, Boris A Matveev, and Maxim A Remennyy. Low voltage co _2-gas sensor based on iii–v mid-ir immersion lens diode optopairs: Where we are and how far we can go? *IEEE sensors journal*, 10(2):225–234, 2009.

[70] Brian K Walsh, David N Crotwell, and Ruben D Restrepo. Capnography/capnometry during mechanical ventilation: 2011. *Respiratory care*, 56(4):503–509, 2011.

[71] Michael B Jaffe. Mainstream or sidestream capnography? *environment*, 4:5, 2002.

[72] Mikel Leturiondo, Sofía Ruiz de Gauna, José Julio Gutiérrez, Digna M González-Otero, Jesus M Ruiz, Luis A Leturiondo, and Purificación Saiz. Waveform capnography for monitoring ventilation during cardiopulmonary resuscitation: The problem of chest compression artifact. In *Cardiac Diseases and Interventions in 21st Century*. IntechOpen, 2019.

[73] John W Severinghaus. Water vapor calibration errors in some capnometersrespiratory conventions misunderstood by manufacturers? *Anesthesiology: The Journal of the American Society of Anesthesiologists*, 70(6):996–998, 1989.

[74] R Fletcher, O Werner, L Nordström, and B Jonson. Sources of error and their correction in the measurement of carbon dioxide elimination using the siemens-elema co2 analyzer. *British Journal of Anaesthesia*, 55(2):177–185, 1983.

[75] International organization for standardization. medical electrical equipment - particular requirements for the basic safety and essential performance of respiratory gas monitors, 2018.

[76] Microstream™ micromedico$_2$ oem module datasheet. `https://www.medtronic.com/covidien/en-us/products/oem-monitoring-solutions/`

microstream-capnography/microstream-micromedico2-oem-module.html. Accessed: 2020-12-24.

[77] Capnostat 5 mainstream co2 sensor datasheet. https://www.pennvet.com/customer/wcm/connect/82e10e56-5c67-4c5e-bda0-214a8140a65f/Bionet_America_Respironics_01-1742-4101194-Capnostat.pdf?MOD=AJPERES&CACHEID=ROOTWORKSPACE-82e10e56-5c67-4c5e-bda0-214a8140a65f-mqy5R2Y. Accessed: 2020-12-24.

[78] Nalinkumar Patel, Julian Carter, Jeremy Walsh, Overend Russell, Calum Mcgregor, Des Gibson, and Ewan Waddell. Capnometer, November 8 2018. US Patent App. 15/534,973.

[79] Juha Aittomäki. Monitoring of co2 exchange during cardiopulmonary bypass: the effect of oxygenator design on the applicability of capnometry. *Perfusion*, 8(4):337–344, 1993.

[80] Michael J Semmens, John S Gulliver, and Anita Anderson. An analysis of bubble formation using microporous hollow fiber membranes. *Water environment research*, 71(3):307–315, 1999.

[81] Jan Olav Høgetveit, Frode Kristiansen, and Thore H Pedersen. Development of an instrument to indirectly monitor arterial pco2 during cardiopulmonary bypass. *Perfusion*, 21(1):13–19, 2006.

[82] Sung Jin Kim and Seok Pil Jang. Experimental and numerical analysis of heat transfer phenomena in a sensor tube of a mass flow controller. *International Journal of Heat and Mass Transfer*, 44(9):1711–1724, 2001.

[83] Led microsensor nt: Led and photodiode datasheet. http://lmsnt.com/. Accessed: 2020-11-20.

[84] Frode Kristiansen, Jan Olav Høgetveit, and Thore H Pedersen. Clinical evaluation of an instrument to measure carbon dioxide tension at the oxygenator gas outlet in cardiopulmonary bypass. *Perfusion*, 21(1):21–26, 2006.

[85] SE Aleksandrov, GA Gavrilov, AA Kapralov, BA Matveev, G Yu Sotnikova, and MA Remennyi. Simulation of characteristics of optical gas sensors based on diode optopairs operating in the mid-ir spectral range. *Technical Physics*, 54(6):874–881, 2009.

[86] Jimena del Castillo, Jesús López-Herce, Martha Matamoros, Sonia Cañadas, Ana Rodriguez-Calvo, Corrado Cechetti, Antonio Rodriguez-Núñez, Angel Carrillo Álvarez, Iberoamerican Pediatric Cardiac Arrest Study Network RIBEPCI, et al. Hyperoxia, hypocapnia and hypercapnia as outcome factors after cardiac arrest in children. *Resuscitation*, 83(12):1456–1461, 2012.